Project Report (Work Package 4)

Hydrogen Impact on NTS Welds

Submitted to:

National Gas Transmission

Principal Investigators:

Jonathan Parker

E-mail: jparker@epri.com

Michael Gagliano

Email: mgagliano@epri.com

March 31, 2026

Electric Power Research Institute

1300 West W.T. Harris Blvd.

Charlotte, NC 28262 USA

Submitted by:

Jonathan Parker

DISCLAIMER OF WARRANTIES AND LIMITATION OF LIABILITIES

This document was prepared as part of a research collaboration between National Gas Transmission plc and the Electric Power Research Institute, Inc. (EPRI) under the terms of the Research and Development Collaboration Agreement dated 12 March 2025. All intellectual property and results arising from this project are owned by National Gas Transmission plc in accordance with that agreement.

Neither EPRI, National Gas Transmission plc, any member of EPRI, any subcontractor, nor any person acting on behalf of any of them:

(A) Makes any warranty or representation whatsoever, express or implied,

(i) with respect to the use of any information, apparatus, method, process, or similar item disclosed in this document, including merchantability and fitness for a particular purpose, or

(ii) that such use does not infringe on or interfere with privately owned rights, or

(iii) that this document is suitable to any particular user's circumstance; or

(B) Assumes responsibility for any damages or other liability whatsoever (including any consequential damages, even if EPRI, National Gas Transmission plc, or any representative has been advised of the possibility of such damages) resulting from your selection or use of this document or any information, apparatus, method, process, or similar item disclosed in this document.

Reference herein to any specific commercial product, process, or service by its trade name, trademark, manufacturer, or otherwise does not necessarily constitute or imply its endorsement, recommendation, or favoring by EPRI or National Gas Transmission plc.

1. Background

To address climate change, the United Kingdom government has set ambitious targets for a low-carbon electrical power network by 2030 [1] and net-zero carbon emissions by 2050 [2]. One technology identified as being critical to enabling these goals is the decarbonisation of industry and power via the use of hydrogen in lieu of natural gas. The critical need for a core hydrogen transmission network linking industrial and power users has been recognised by the National Infrastructure Commission (NIC), the UK Department for Energy Security and Net Zero, and the Climate Change Committee (CCC). Project Union is a major national infrastructure programme by National Gas to design and build a hydrogen transmission network within Great Britain. The network will comprise both repurposed natural gas pipelines and new build sections, initially at a regional level linking hydrogen producers, users and storage providers, before ultimately forming a 1500-mile hydrogen backbone across Great Britain.

In accordance with hydrogen transmission standards such as ASME B31.12 [3] and IGEM/TD/1 Supplement 2 [4] the design of new pipelines and the repurposing of natural gas assets for hydrogen service requires consideration of the effects of hydrogen embrittlement. Engineering assessments including the use of fracture mechanics approaches such as those described in BS 7910 [5] or API 579-1/ASME FFS-1 [6] are mandated to permit operation at high design factors. For pipeline systems, the locations of most interest for these engineering assessments are the pipe seam and girth welds, as these are expected to contain the largest and therefore most potentially injurious defects, in addition to having the potential for complexities such as residual and/or misalignment stresses. As a result, data relating to the condition and quality of welds alongside in-hydrogen material property data is required to conduct appropriate assessments. Consideration should be given to the variety of different welding techniques, materials and quality measures adopted during construction of the pipeline network, which can comprise a multitude of different pipe manufacturers and welding contractors over the history of the asset.

Furthermore, the material characterisation of welded microstructures in high-pressure hydrogen containing environments is very challenging from an experimental testing standpoint and existing standards and guidelines such as ANSI/CSA CHMC-1 [7] and the EPRG Best Practice Guide [8] only provide limited guidance on the testing of welded specimens.

National Gas have undertaken an extensive programme of in-hydrogen fracture toughness and fatigue crack growth testing of pipe materials and associated seam and girth welds extracted from the UK National Transmission System (NTS) to feed into repurposing assessments of the NTS. This report provides pre-test metallography of selected welds and focuses on detailed post-test fractographic investigations of fracture toughness specimens tested in gaseous hydrogen. These examinations were undertaken to characterize specific features of the crack path and offer the opportunity to explain apparent differences of the in-hydrogen fracture of pipeline steel weld microstructures. Detailed post-test characterization of the transition from in-air fatigue cracking to the in-hydrogen testing provides the potential for improved understanding of the factors affecting the fracture behaviour.

2. Introduction and Context

The overall work program for the project ‘Hydrogen Impact on NTS Welds’ was organized by specific tasks or work packages (WP). It was agreed that each of the work packages would be reported individually. However, because it was recognized that the learnings and outcomes of the individual tasks required integration to provide an overall appreciation of potential issues, this document provides summaries of key tasks from the individual work packages as well as a discussion of issues associated with repurposing the NTS for hydrogen service. In line with EPRI’s preferred approach to establish evidence of the pedigree of the steels used, the first technical chapter of the report provides information from metallurgical characterization of selected components supplied by NTS. The following sections then summarize findings from the project:

- Review and comment on procedures selected from those provided by NTS,
- Post-test Characterisation of Weld Fracture Toughness Specimens,
- Analysis of the Fracture Toughness Data, and
- A discussion section considers an overall assessment of the results of the study with particular emphasis on potential influences of repurposing to include the transmission of hydrogen.

Recommendations are provided which outline potential future work which should be undertaken to reduce uncertainty in assessing future performance.

Supporting information is provided as References and these source documents should be reviewed as necessary.

3. Metallurgical Background and Testing Methods

Sections from three steel line pipes containing seam and girth welds were provided by National Gas Transmission plc. Two of these steels (designated X60A and X60B) were API 5L X60 grade, both of which had been removed after service in natural gas. The third steel was an API 5L X80 grade that had not been in service. Pipe section X60A is a vintage steel that was manufactured and installed around 1970 and has a 762 mm (30 in) outer diameter (OD) and a 12.7 mm (0.500 in) wall thickness (WT). Pipe section X60B is a modern line pipe steel that was manufactured and installed in 1998 and has a 1050 mm (41.3 in) OD and 14.3 mm (0.562 in) wall thickness. The X80 steel pipe was manufactured in 2007 but never installed in the NTS; the girth weld in this section was manufactured in 2022. The nominal pipe OD and wall thickness are 1220 mm (48 in) and 20.6 mm (0.811 in). Base metal microstructures of X60A and X60B consisted of pearlite in ferrite, while the X80 steel microstructure was comprised of acicular ferrite and bainite [9]. The base metal composition of each steel is presented in Table 1.

Table 1: Chemical compositions of the three pipeline steels evaluated (wt%)

Material	C	Mn	P	S	Nb+V+Ti	Cu	Ni	Fe
X60A	0.178	1.30	0.016	0.043	0.096	0.02	0.04	Bal.
X60B	0.086	1.17	0.016	0.017	0.045	0.01	0.02	Bal.
X80	0.065	1.80	0.016	<0.001	0.070	0.19	0.20	Bal.

Vickers microhardness testing was performed using a load of 0.5 kgf (HV0.5), a 13 second dwell time and an indent-to-indent spacing of 250 µm. The measurements were processed to produce maps of the through-thickness hardness distribution across each of the welds with data from the base metal and heat affected zones (HAZs) included.

A Bruker M4 Tornado micro-x-ray fluorescence (µ-XRF) chemical analyser was used to map the distribution of elemental constituents and quantify chemical homogeneity in the base metal and welds of all three pipes. Testing parameters for all three samples were standardized; these used an accelerating voltage of 50 kV, an anode current of 575 µA, a pixel (and spot) size of 20 µm, and an Al/Ti 100/25 sandwich filter.

3.1. Metallographic Characterization

3.1.1. Pipe X60A

3.1.1.1. X60A Girth Weld

A macrograph through the girth weld of X60A is shown in Figure 1. It appears that the girth weld was produced with multiple passes using a predominantly weaved technique. In general, manufacture of welds using weaved passes introduces variability and therefore uncertainty into the heat input and thermal distribution and thus influences the microstructures present.

Consideration of Figure 1 shows differences in the width of the heat affected zone (HAZ) on opposite sides of the weld. The pattern of weld beads also indicates a relatively thick capping run with local stress concentrations at the edge of the weld metal. The microstructure in the base metal was a mixture of ferrite and pearlite. Significant numbers of inclusions elongated along the axial direction of the pipe were also observed. The appearance indicated that these inclusions were primarily manganese sulfide (MnS).

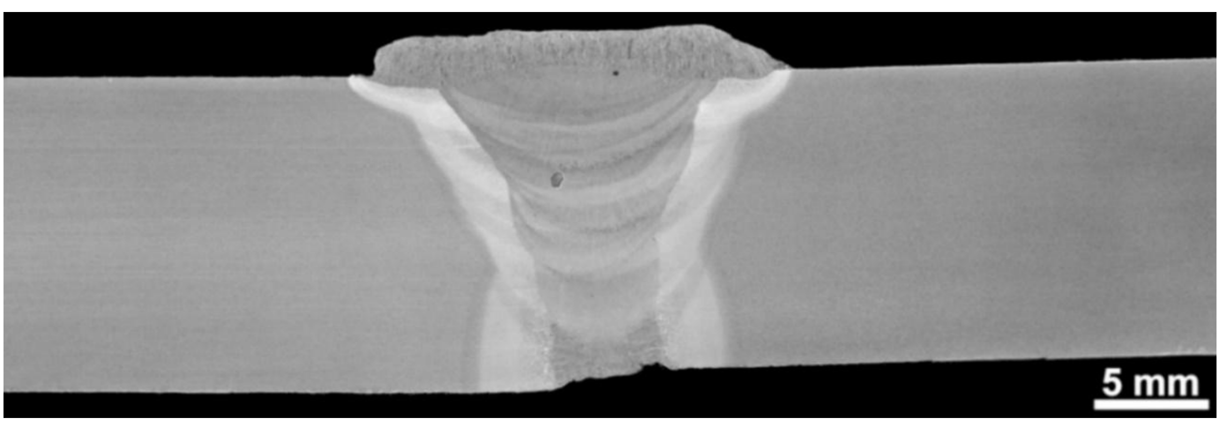

Figure 1: Macrograph of the Structures Present in the Girth Weld of the X60A steel pipe.

The microstructures in the weld HAZ were more complex. A typical optical micrograph of a traverse from the weld near the fusion line to the base metal is shown in Figure 2. The thermal cycles introduced during welding resulted in differences in the microstructure, with higher peak temperatures and faster cooling rates near the fusion line to temperatures which do not significantly alter the base structure about 2 mm away. In the present case, no martensite was observed in the optical microscope. It is apparent that the inclusion stringers are present even very close to the weld fusion line, indicating that temperatures attained in the heat affected zone during welding were insufficient to dissolve the MnS stringers. Two porosity type weld metal defects are shown in Figure 1.

Figure 2: Etched cross section showing the weld fusion line and the variability of the microstructure in the HAZ of the X60A girth weld. The horizontally aligned features in the HAZ adjacent to the weld fusion line are MnS stringers.

It is often the case that welding leads to local variations in composition, both within the weld and between the weld and base metal. To obtain an overview of the distribution of selected elemental constituents, µ-XRF analysis was undertaken; the results for weld X60A are presented in Figure 3. Of the eight maps shown, the first shows the distribution of iron (Fe) across the weld. The elements highlighted in the remaining seven images are manganese (Mn), molybdenum (Mo), nickel (Ni), niobium (Nb), copper (Cu), vanadium (V) and chromium (Cr).

Each map shows the relative concentration of the elements present and as such are a useful approach for showing variations. It is apparent that the fill passes show higher levels of molybdenum than the root passes. In contrast, the root passes showed higher levels of Ni, Cu and Cr than were measured in the fill layers. However, even at the high end the compositions were about 0.05 wt%. To provide a semi-quantitative assessment of Mo the high-end levels were about 0.5 wt% whereas the lower levels were about 0.004 wt%.

Hardness measurements are often used to complement metallographic information. EPRI has used hardness and microhardness maps of welds to highlight local variations. These variations do not by themselves identify a microstructural constituent but clearly these maps are a useful tool to visualize microstructural heterogeneity. The hardness map from girth weld X60A is shown in Figure 4. The data show that there are hardness variations in the base metal and more particularly in the weld and HAZ. The values measured in the HAZ appear to be highest towards the root and under the final capping pass. In these regions individual measurements exceed 250 HV0.5. It is also interesting that the lowest values in the weld metal are measured in the region below the capping pass where values of around 160 HV0.5 were recorded.

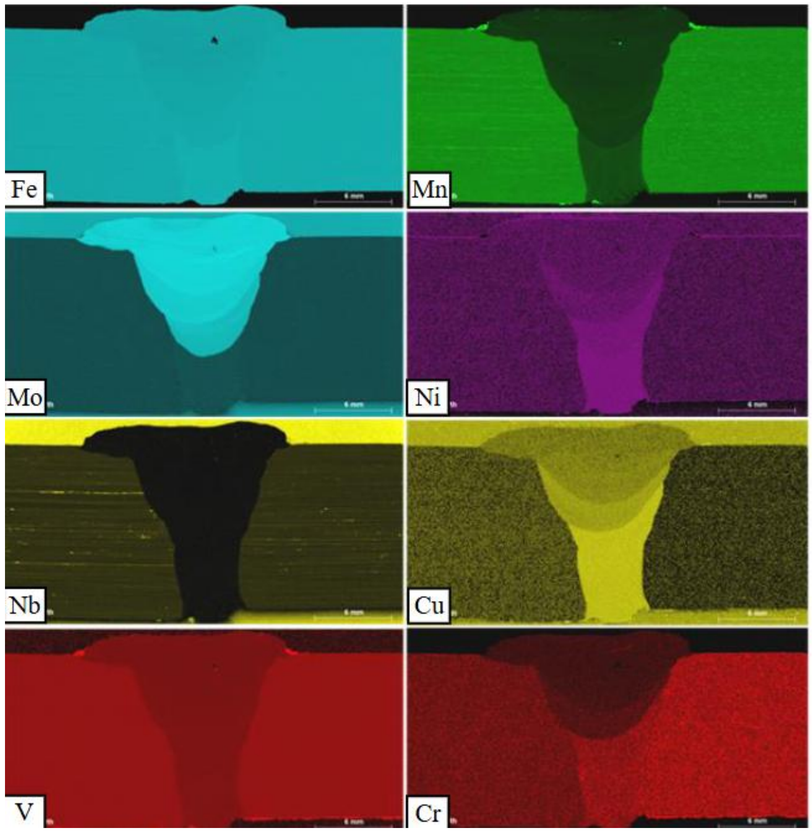

Figure 3: μ-XRF map showing the distribution of Fe, Mn, Mo, Ni, Nb, Cu, V, and Cr in the X60A girth weld. The brighter colours indicate higher concentrations of specific elements.

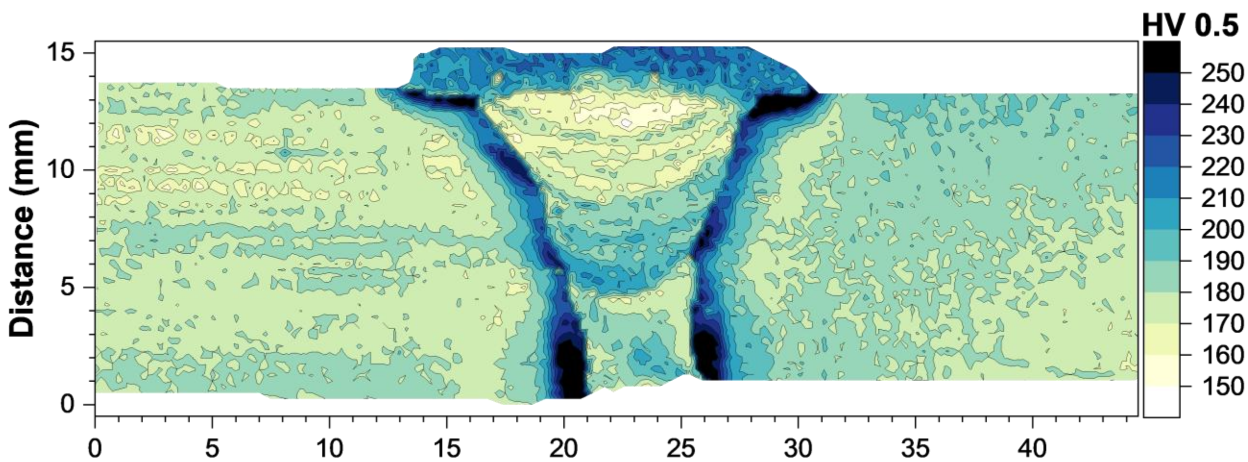

Figure 4: Through-thickness microhardness map measured from the cross section taken from the girth weld of the X60A steel pipe.

3.1.1.2. X60A Seam Weld

A macrograph through the seam weld of X60A is shown in Figure 5. It appears that the weld was produced with two passes, the first bead deposited from the outside of the pipe and the second from the inside.

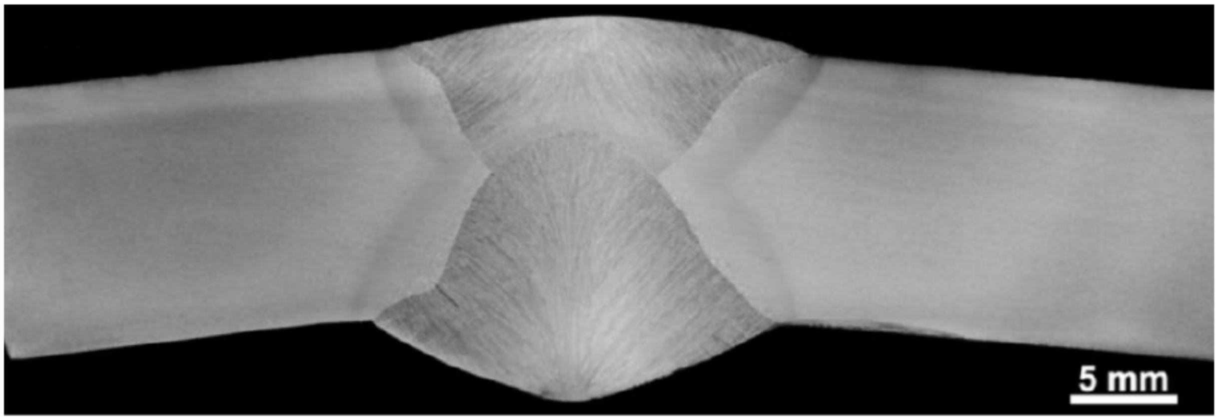

Figure 5: Macrograph of the structures present in the seam weld of the X60A steel pipe.

The general appearance of the beads was consistent with submerged arc welding. As is typical for submerged arc welds, the relatively fast cooling rate results in predominantly columnar grain structure in the weld metal. In the present weld, defects were detected, one in each bead. These defects are shown in more detail in Figure 6. The defects appeared to be formed just inside the weld metal and appeared to be predominantly intergranular in nature.

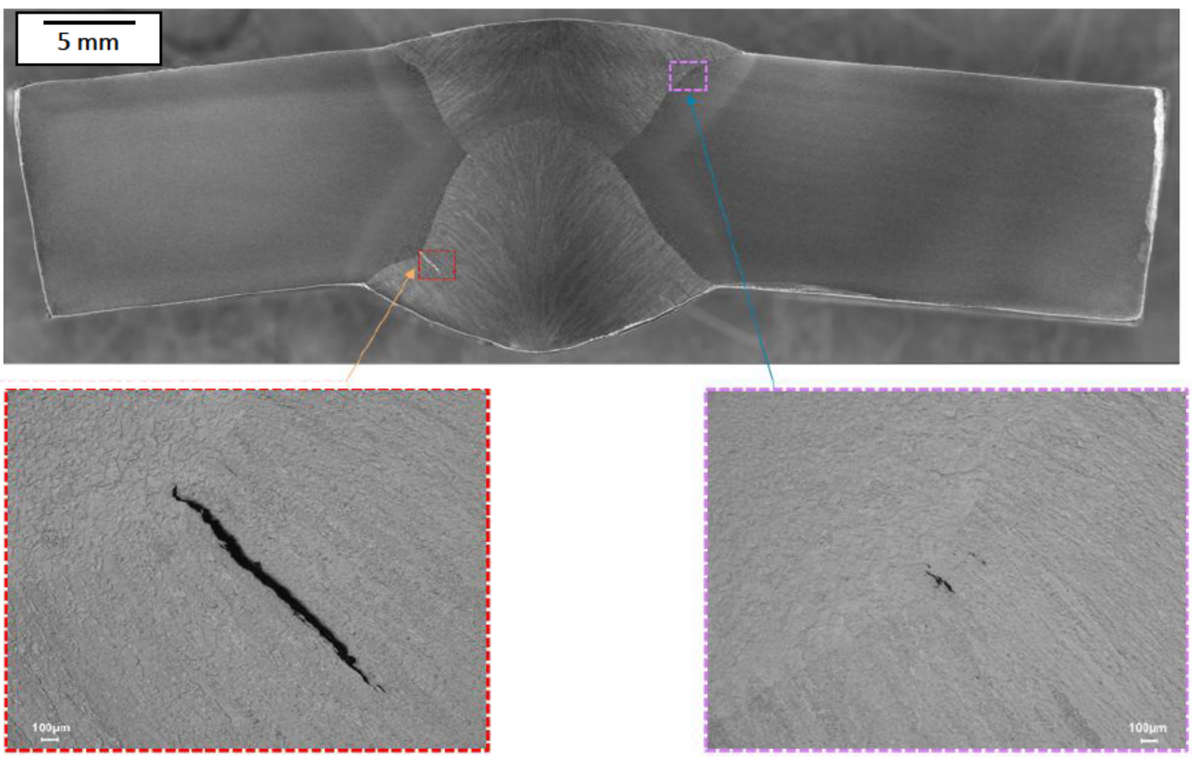

Figure 6: Macrograph of the seam weld of the X60A steel pipe showing the locations of microdefects in the weld metal.

To obtain an overview of the distribution of selected elemental constituents, µ-XRF analysis was undertaken; the results for the seam weld in pipe X60A are presented in Figure 7. Of the eight maps shown, the first shows the distribution of iron (Fe) across the weld. The elements highlighted in the remaining seven images are manganese (Mn), molybdenum (Mo), nickel (Ni), niobium (Nb), copper (Cu), vanadium (V) and chromium (Cr). Each map shows the relative concentration of the elements present. The resolution of the elements was set to identify small differences and even using high sensitivity scans only small variations were identified. The greatest differences were in the levels of Mn and Cu, however the values obtained were within the scatter that would be expected from welds manufactured using the same consumables and process.

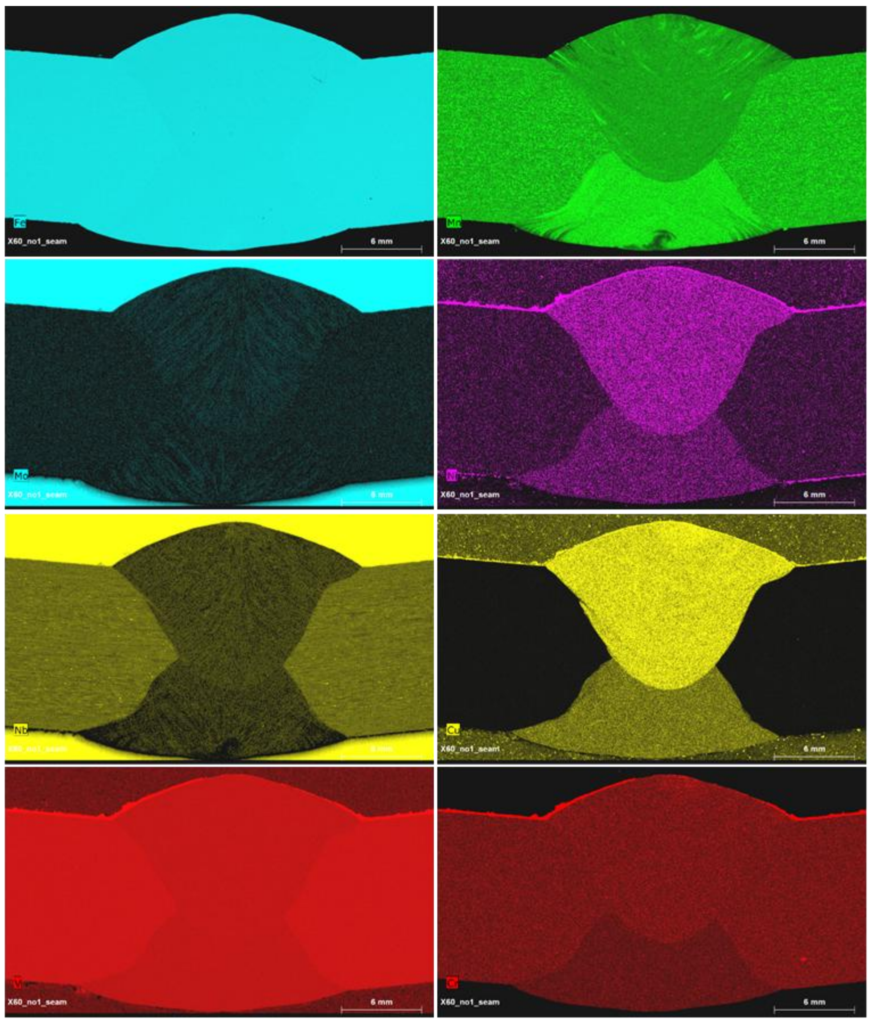

Figure 7: μ-XRF map showing the distribution of Fe, Mn, Mo, Ni, Nb, Cu, V, and Cr in the X60A seam weld. The brighter colours indicate higher concentrations of specific elements.

Hardness measurements are often used to provide information which supplements the results of metallographic observations. EPRI has used hardness and microhardness maps of welds to highlight local variations. These variations do not by themselves identify a microstructural constituent but clearly these maps are a useful tool to visualize microstructural heterogeneity. The hardness map from the seam weld X60A is shown in Figure 8. The data show that there are hardness variations in the base metal with the values obtained in the range 150 to 170 HV0.5. The hardness of the weld was higher with variations in the range 200 to 250 HV0.5. The values measured in the HAZ, Figure 8, appear to be significantly lower than those measured in the X60A girth weld, Figure 4. In the HAZ of the seam weld the individual measurements are all approximately 175 HV0.5. It is also interesting to note that the hardness distributions show that the heat input from the second bead tempered the hardness of the first bead. The pattern of hardness values demonstrates the influence that cooling rate and thermal cycles have on the constituent structure and properties.

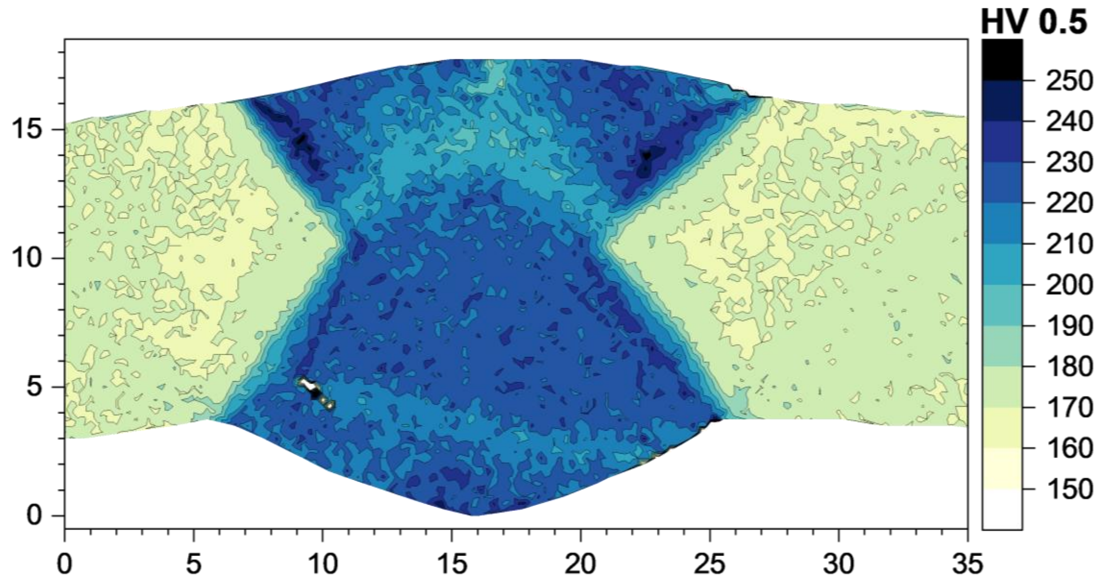

Figure 8: Through-thickness microhardness map across the seam weld of X60A steel.

3.1.2. Pipe X60B

3.1.2.1. X60B Girth Weld

A macrograph through the girth weld of X60B is shown in Figure 9. It appears that the girth weld was produced with multiple passes using a predominantly weaved technique. In general, manufacture of weld using weaved passes introduces uncertainty into the heat input and thermal distribution.

Consideration of Figure 9 shows differences in the width of the heat affected zone (HAZ) on opposite sides of the weld. The pattern of weld beads also indicates a relatively thick capping run with local stress concentrations at the edge of the weld metal. It appears that this capping bead resulted in significant heating of the preexisting weld, HAZ and base metal. The microstructure in the base metal was a mixture of ferrite and pearlite. Some inclusions elongated along the axial direction of the pipe were observed but the extent appeared to be lower than that observed in X60A. The appearance indicated that these inclusions were primarily manganese sulfide (MnS). The variation of the level of Mn in the base metal is evident from the results of the μ-XRF maps shown in Figure 10.

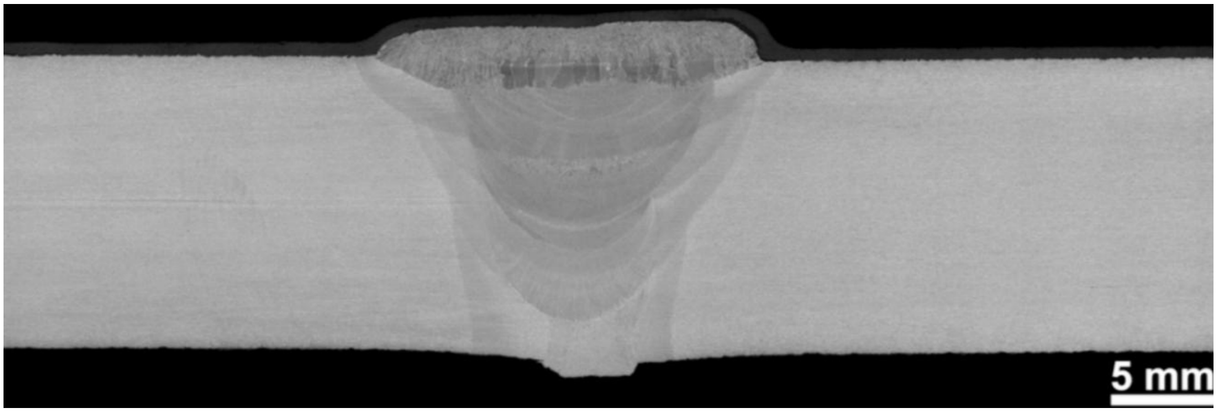

Figure 9: Macrograph of the structures present in the girth weld of the X60B steel pipe.

To obtain an overview of the distribution of selected elemental constituents, μ-XRF analysis was undertaken; the results for girth weld X60B are presented in Figure 10. Of the eight maps presented, the first shows the distribution of iron (Fe) across the weld. The elements highlighted in the remaining seven images are manganese (Mn), molybdenum (Mo), nickel (Ni), niobium (Nb), copper (Cu), vanadium (V) and chromium (Cr). Each map shows the relative concentration of the elements present and as such are a useful approach for showing variations. It is apparent that the fill passes show higher levels of Ni, Cu than the root passes. However, even at the high end the compositions of Ni were about 0.04 wt%, Figure 10.

The hardness map from girth weld X60B is shown in Figure 11. The data show that there are hardness variations in the base metal and more particularly in the weld and HAZ. In this weld, while the cap and weld root show relatively high hardness, values in the HAZ are comparatively lower. Thus, in some locations the hardness of the HAZ is at or below 150 HV0.5, indicating that the recorded values are lower than those of the base metal. This observation is consistent with the welding process having caused temperatures and cooling rates sufficient to soften the steel. Softening of this type could be a concern for in-service performance if the strength is reduced to a level below that required by the specification for the specified grade.

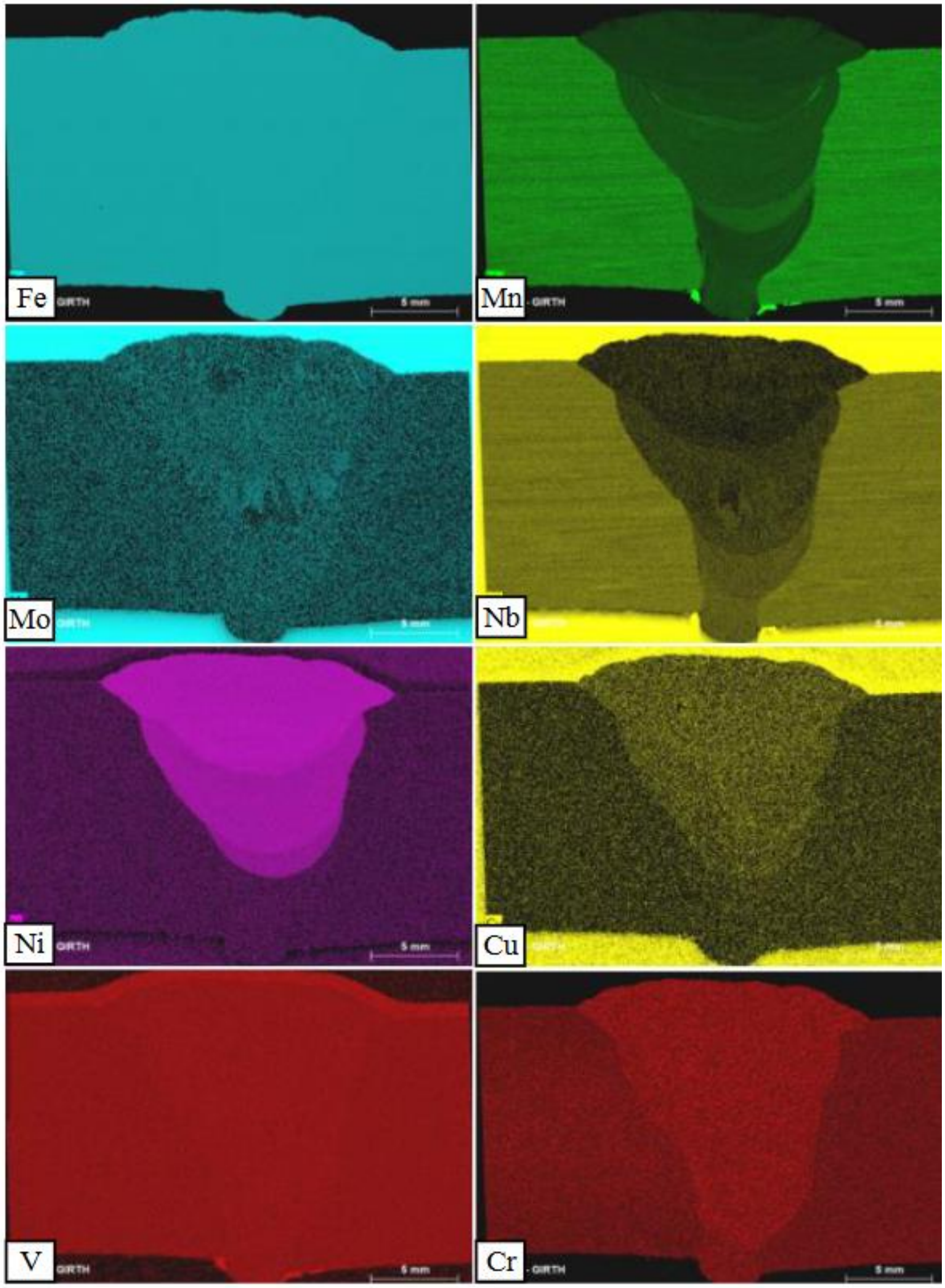

Figure 10: μ-XRF map showing the distribution of Fe, Mn, Mo, Ni, Nb, Cu, V, and Cr in the X60B girth weld. The brighter colours indicate higher concentrations of specific elements.

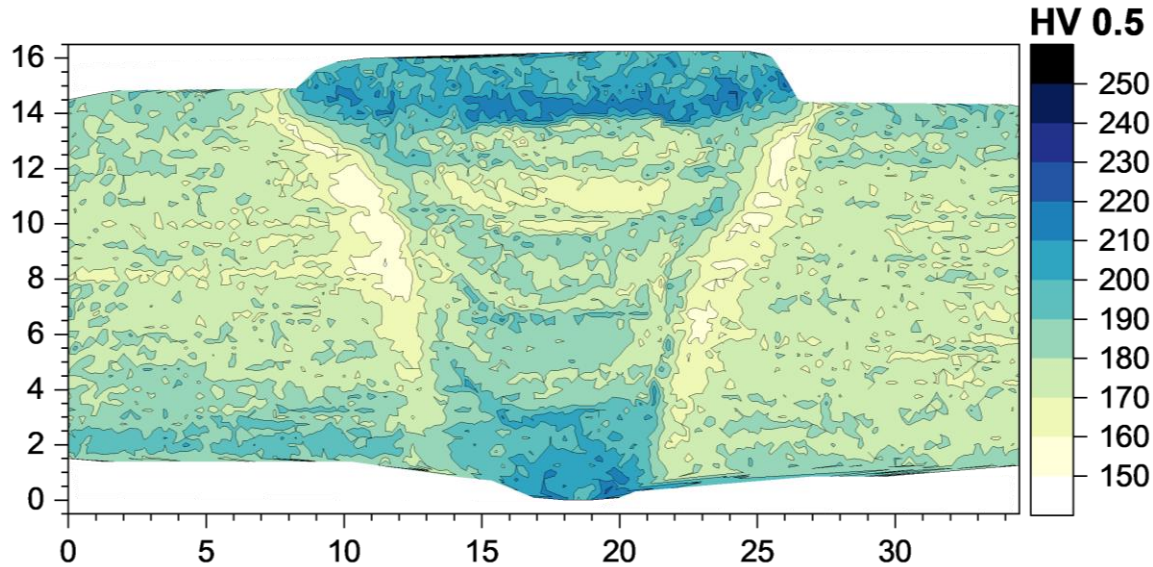

Figure 11: Through-thickness microhardness map across the girth weld of X60B steel.

3.1.2.2. X60B Seam Weld

A macrograph through the seam weld of X60B is shown in Figure 12. It appears that the weld was produced with two passes, the first bead deposited from the inside of the pipe and the second from the outside. The general appearance of the beads was consistent with submerged arc welding. As is typical for submerged arc welds, the relatively fast cooling rate results in predominantly columnar grain structure in the weld metal.

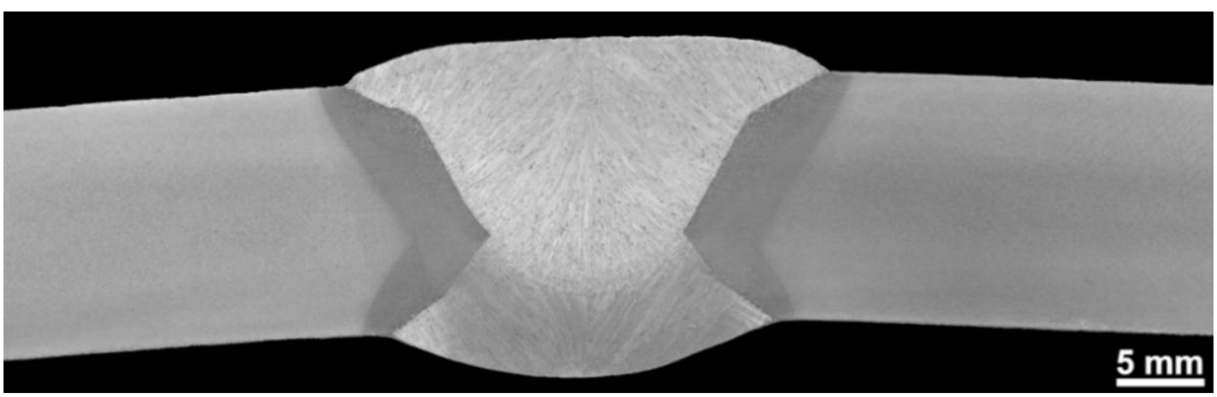

Figure 12: Macrograph of the structures present in the seam weld of the X60B steel pipe.

To obtain an overview of the distribution of selected elemental constituents, μ-XRF analysis was undertaken; the results for the seam weld in X60B are presented in Figure 13. Of the eight maps shown, the first shows the distribution of iron (Fe) across the weld. The elements highlighted in the remaining seven images are manganese (Mn), molybdenum (Mo), nickel (Ni), niobium (Nb), copper (Cu), vanadium (V) and chromium (Cr). Each map shows the relative concentration of the elements present and as such are a useful approach for showing variations. It is apparent that the composition of the welds is generally uniform. Of note is the fact that the weld metal fill passes show higher levels of Mn and Mo than the base metal. Both of these elements increase strength (among other things) and are often used to ensure the strength of the weld is at least equal to (and generally higher) that of the base metal. The relative values were Mn about 1.0 wt.% in the base metal and 1.25 wt% in the weld. For Mo, the values were about 0.16 wt.% measured in the weld with no significant level in the parent.

The composition in the weld beads is consistent with the same consumable being used.

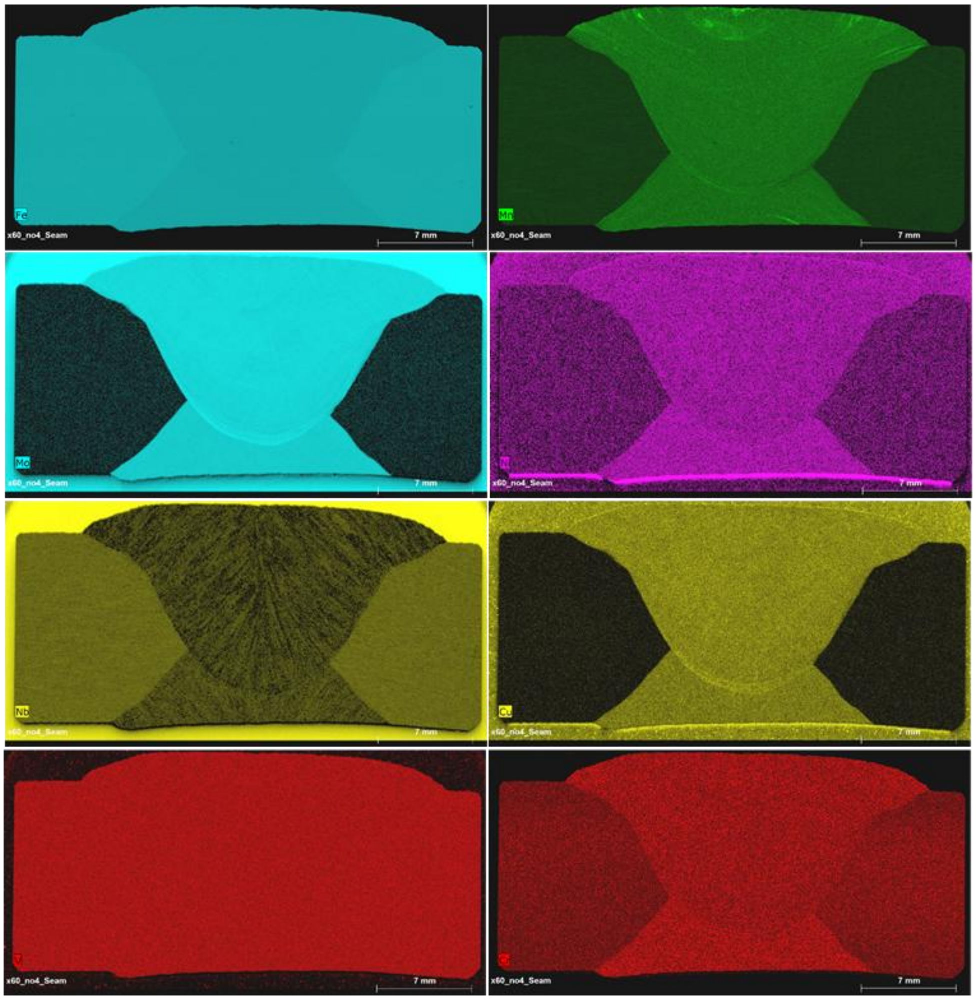

Figure 13: μ-XRF map showing the distribution of Fe, Mn, Mo, Ni, Nb, Cu, V, and Cr in the X60B seam weld. The brighter colours indicate higher concentrations of specific elements.

The hardness map from seam weld X60B is shown in Figure 14. The data show that there are hardness variations in the base metal and more particularly in the weld and HAZ. In this weld, while the second bead shows significantly greater hardness than the first. This variation could be a consequence of tempering from the thermal cycles of bead 2. The hardness in the weld metal of the second bead is in the range 200 to 240 HV0.5. The values in the HAZ are significantly lower. Thus, in the majority of locations the hardness of the HAZ is at or below 150 HV0.5. Clearly these recorded values are lower than those of the base metal. This observation is consistent with the welding process having caused temperatures and cooling rates sufficient to soften the steel.

Softening of this type could be a concern for in-service performance if the strength is reduced to a level below that required by the specification for the specified grade.

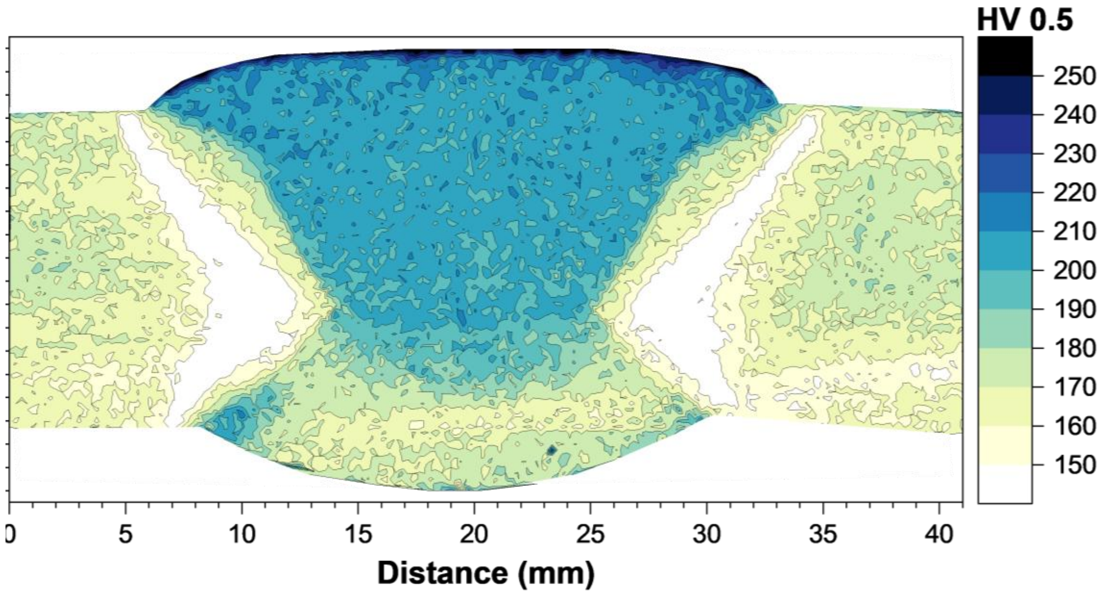

Figure 14: Through-thickness microhardness map across the seam weld of X60B steel.

3.1.3. Pipe X80 Girth Weld

3.1.3.1. X80 Girth Weld

A macrograph of the girth weld in X80 is shown in Figure 15. It appears that the girth weld was produced using a variety of beads. The regions nearest to the OD have the appearance of being produced using stringer bead with mid-wall and other regions showing a predominantly weaved technique. Based on the appearance of the individual layers there appears to be a significant difference between the outer two thirds and the inner one third of the fill. There also appears to be variability in the heat input between parts of the HAZ. The variability is consistent with the fact that welding using weaved passes introduces uncertainty into the heat input and thermal distribution. There is a weld defect present in the weld metal.

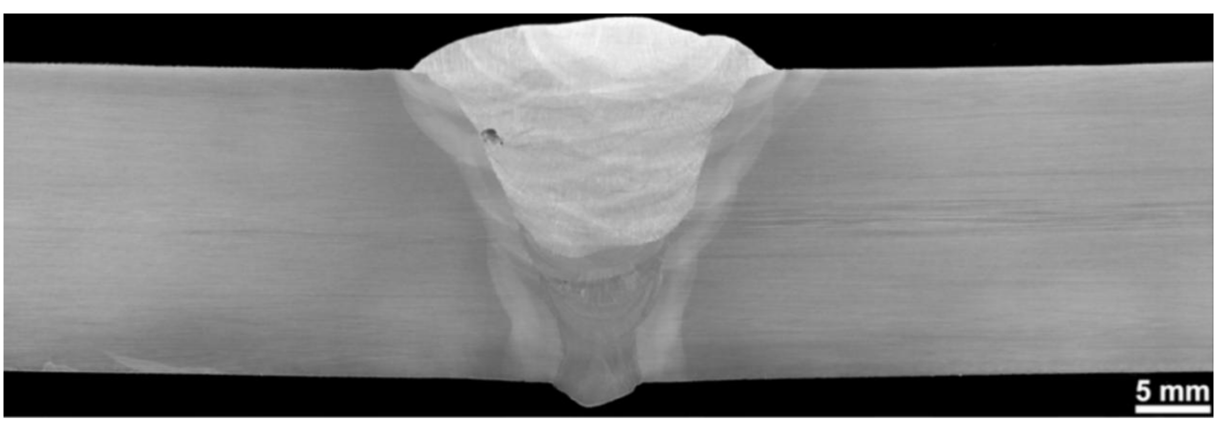

Figure 15: Macrograph of the structures present in the girth weld of the X80 steel pipe.

The results for μ-XRF analysis for selected elements in the girth weld X80 obtained in the scanning electron microscope are presented in Figure 16. The distribution of Ni, Mn and V show significant separation between the outer two thirds and the inner one third of the fill pass. In this weld the outer beads showed Mn of above about 1.0 wt.% whereas the inner beads had measured levels of less than 0.7 wt%. The variation in Ni was about 1.4 wt.% for the outer beads and less than 0.06 wt.% for the inner beads. While little V was recorded in the outer beads the inner passes showed 0.03 wt.%. As noted for the other joints there are distinct differences in composition between the different weld beads and the base metal.

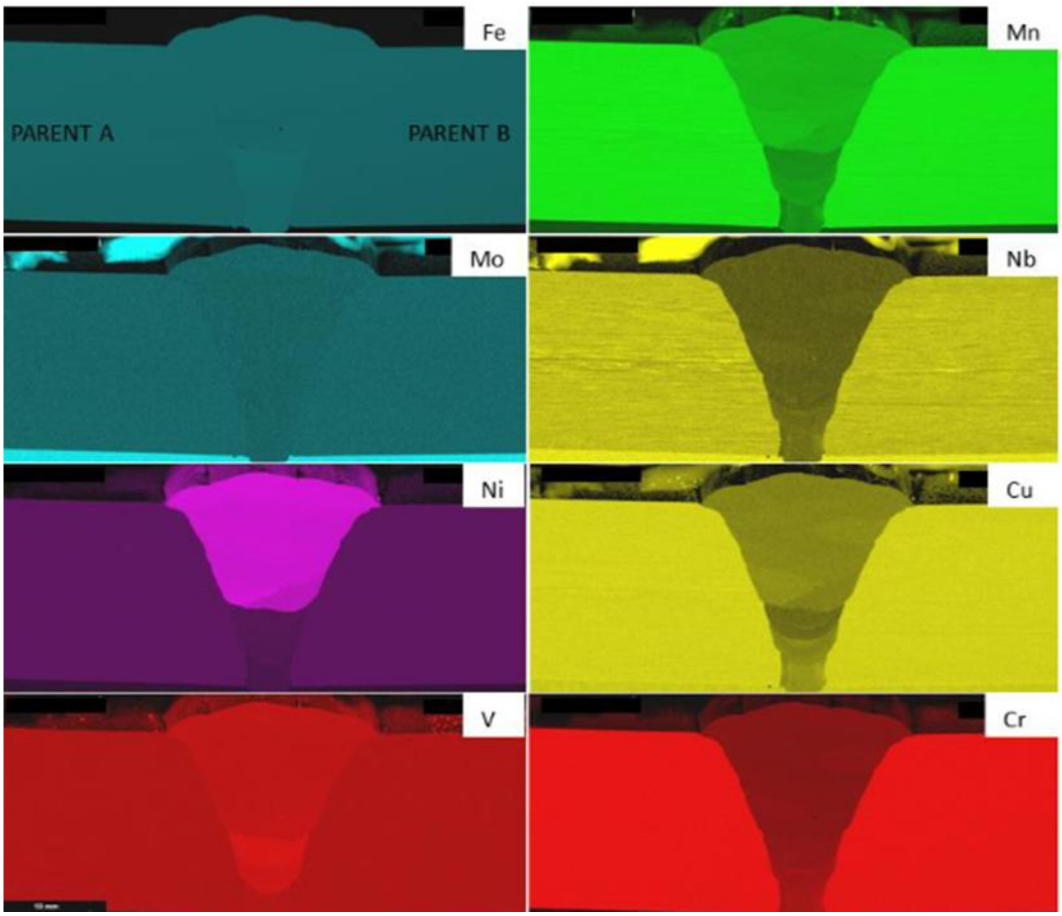

Figure 16: μ-XRF map showing the distribution of Fe, Mn, Mo, Ni, Nb, Cu, V, and Cr in the X80 girth weld. The brighter colours indicate higher concentrations of specific elements.

The hardness map from girth weld of X80 is shown in Figure 17. The data shows that there are hardness variations in the base metal and more particularly in the weld and HAZ. In this weld there is a significant difference in hardness between the outer two thirds and the inner one third of the fill, with the inner one third exhibiting an appreciably lower hardness. The cap pass clearly shows the highest hardness in the weld metal with measured values in excess of 250 HV0.5. It is interesting to note that the hardness in the heat affected zone immediately adjacent to the weld fusion line is consistently at or near the upper limit of the recommended hardness limit recommended by ASME B31.12 (i.e. at or above 250 HV0.5), regardless of the location through the thickness.

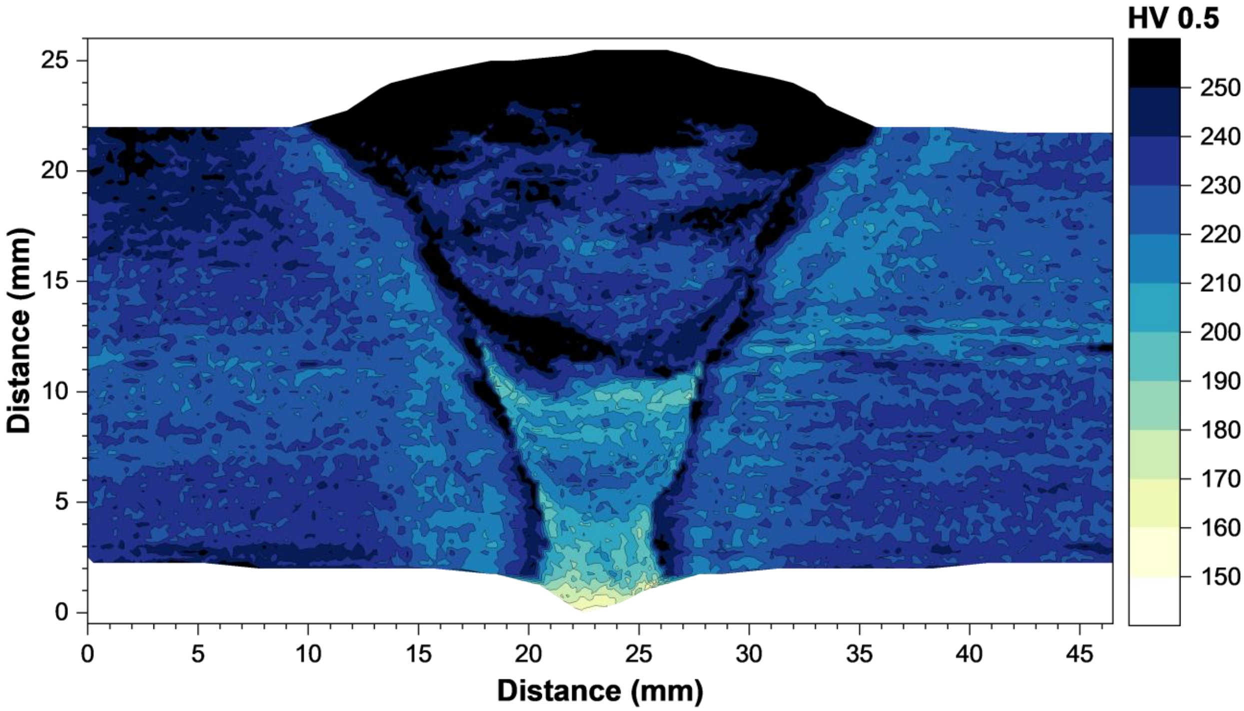

Figure 17: Through-thickness microhardness map across the girth weld of X80 steel.

3.1.3.2. X80 Seam Weld

A macrograph through the seam weld of X80 is shown in Figure 18. It appears that the weld was produced with two passes, the first bead deposited from the inside of the pipe and the second from the outside.

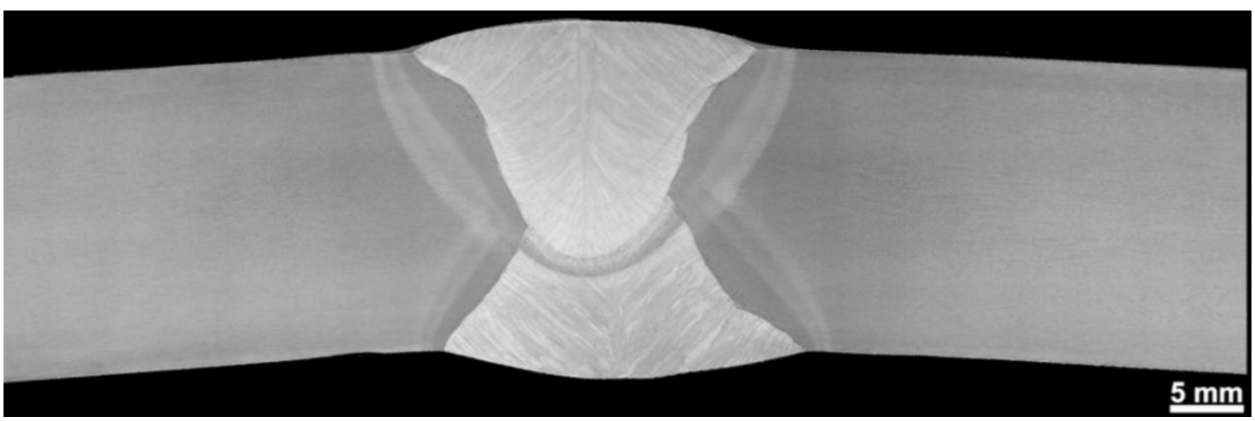

Figure 18: Macrograph of the Structures Present in the Seam Weld of the X80 steel pipe.

The general appearance of the beads was consistent with submerged arc welding. As is typical for submerged arc welds, the relatively fast cooling rate results in predominantly columnar grain structure in the weld metal. The size of the HAZ for both beads is relatively wide, indicating a high heat input.

The results for μ-XRF analysis for selected elements in the seam weld of X80 obtained in the scanning electron microscope are presented in Figure 19.

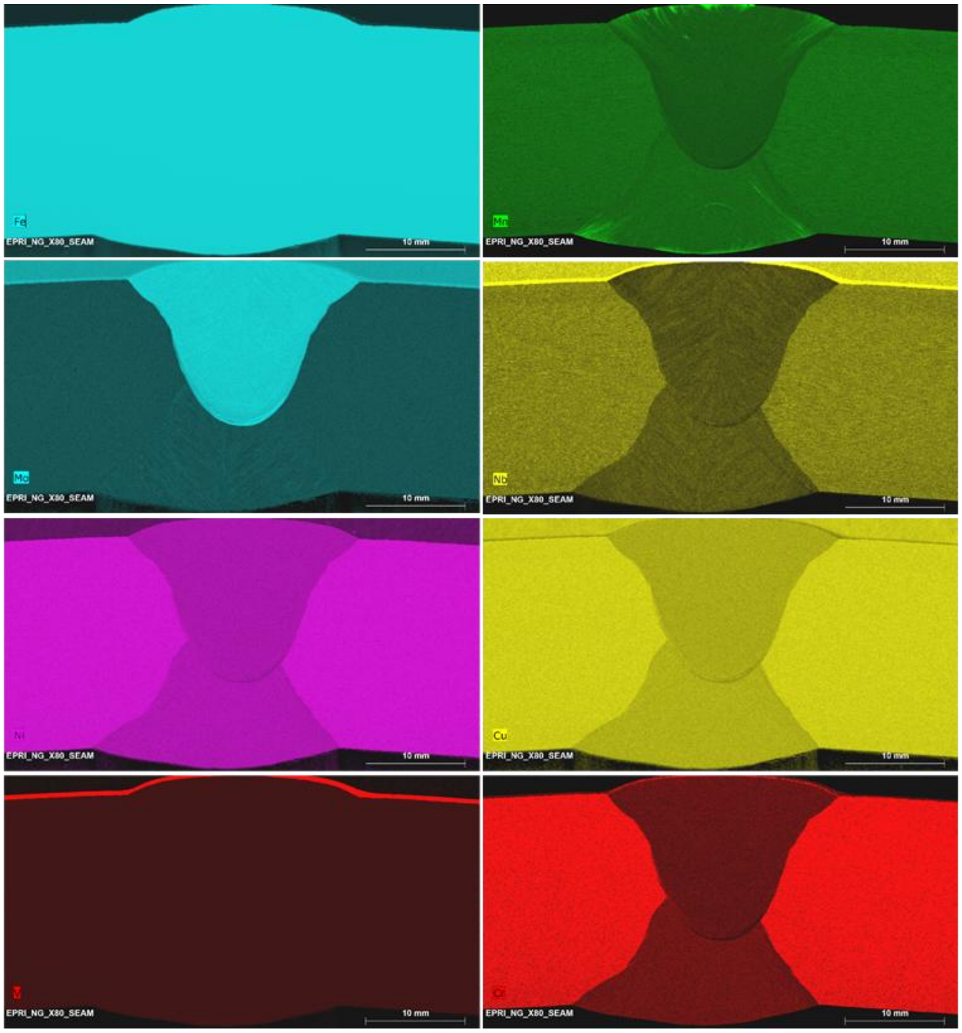

Figure 19: µ-XRF map showing the distribution of Fe, Mn, Mo, Ni, Nb, Cu, V, and Cr in the X80 seam weld. The brighter colours indicate higher concentrations of specific elements.

The most significant variation in composition was recorded for the Mo levels, the first bead (from the inside) contained less than 0.005 wt% whereas the second bead (from the outside) revealed about 0.12 wt%. The higher Mo level recorded was significantly greater than the level in the base steel.

The hardness map from seam weld X80 is shown in Figure 20. The data show that there are hardness variations in the base metal and more particularly in the weld and HAZ. In this weld there is a significant difference in hardness between the first, inner bead and the second, outer bead. The inner bead clearly shows the highest hardness in the weld metal with measured values more than 250 HV0.5. It is interesting to note that the hardness in the heat affected zone immediately adjacent to the weld fusion line is at the lowest level recorded in this weld, between 190 and 200 HV0.5. The hardness in the base was variable with the highest values recorded being about 230 HV0.5.

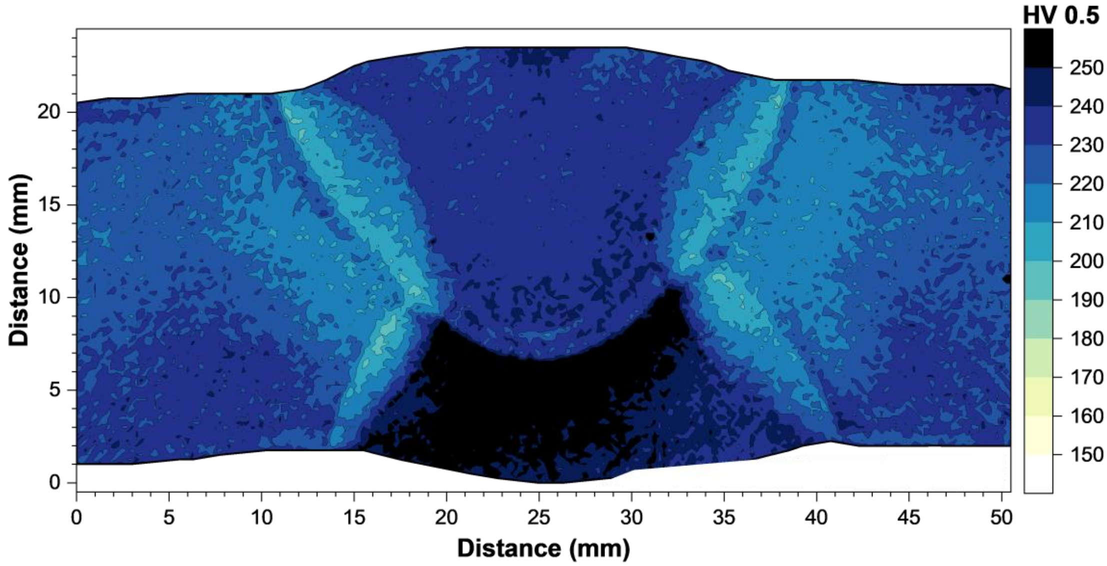

Figure 20: Through-thickness microhardness map across the seam weld of X80 steel.

3.2. Summary of Key Findings from the Metallographic Characterization

It is apparent from the metallurgical examination of selected weld samples from line pipe that there are many complexities. These include:

- Variations in the way the weld beads were deposited. This was even true for the submerged arc seam welds where in two cases the initial bead was laid on the inside of the pipe. Generally, the evidence was that the seam weld beads were laid using the same consumable. In some locations the measured hardness values were above 250 HV0.5. [redacted] [8].
- The HAZ measured hardness was variable between the different welds. In the X60B seam weld, values were below 140 HV0.5. Using a standard hardness to tensile strength conversion table for carbon and low alloy steels in ISO 18265 [10], a hardness value of 140 HV correlates to an approximate tensile strength of 450 MPa (65 ksi). API 5L 46th Edition [11] indicates a minimum required tensile strength of 520 MPa (75.4 ksi) for X60 line pipe. Thus, hardness testing suggests that the strength within the heat affected zone may be below that of the base steel grade.
- The metallographic cross section from the seam weld in pipe X60A revealed weld metal defects close to the fusion line. The largest defect was about 2.5 mm in linear dimension. Defects of this size and type should not be present.
- Compositional differences were noted between the base metal and weld consumables. Such differences, coupled with welding thermal cycles will lead to local heterogeneity in mechanical properties, resulting in a metallurgical notch being established. Due to these highly localized effects, simple, laboratory-based tests conducted on specimens removed from weld and heat affected zones are generally insufficient to represent the actual performance of a component with significant.
- The base steel microstructure was typically ferrite and pearlite. Some banding of the microstructure was noted. Manganese sulfide inclusion stringers were observed with the highest amount identified being in X60A.

4. Review of NTS Procedures (WP1)

National Gas Transmission (NGT) provided EPRI with access to available documentation related to the manufacture and fabrication of the pipeline, materials specification at the time of manufacturer, and quality assurance reports, where available. Weld procedure specifications for girth welding were considered, based on steel grade and/or thickness for all relevant line pipe.

The examples provided in this section aim to highlight selected information relevant to the specifications used for original construction. It was not possible to review all of the information available. Therefore, this overview evaluates areas where the approaches, which were allowed at the time of the manufacture and installation of pipelines for natural gas service, may be of concern when considering repurposing the same pipeline for the transmission of hydrogen.

A very wide range and large number of documents have been considered, and the EPRI report cannot provide a detailed summary of all the available information. Thus, the source documents should be reviewed for definitive information. A document manifest was produced by NGT to identify the individual reference documents. The manifest has been used to link comments to document identification.

4.1. Commentary on records related to parent steel

4.1.1. Pipe Metallurgy

Based on a recent review of historical information [12] all pipes made in the UK before 1975 were manufactured using ingot casting, followed by production using controlled rolling, normalized rolling or normalized plate. Typically, these processing methods resulted in predominately ferrite / pearlite microstructures with the highest grade being X52. The plate of this vintage had lower cleanliness and higher levels of carbon than steel made using modern methods. These factors resulted in lower performance in drop weight tear testing (DWTT) than would be achieved with more modern steel. It should be noted that higher grades such as X60 supplied from non-UK pipe mills, were used on the NTS from the late 1960s onwards.

From about 1975 improved manufacturing methods introduced in the UK, such as the use of continuous casting, thermo-mechanical rolling and improved composition, allowed the maximum grade steel to achieve properties up to those defined for X65 grade. These steels typically had carbon in the range 0.10 – 0.17 wt% with higher degrees of cleanliness. Subsequently, further controls on composition and the introduction of thermomechanically controlled processing (TMCP) allowed higher grades of line pipe steel to be manufactured in the UK.

Typical pipe dimensions were 914 mm outside diameter and 17.6 mm wall thickness. About 96% of the pipe was made using Submerged Arc (SA) welding process; with about 1% made using Electric Resistance Welding (ERW) and about 3% was seamless. In general, the aim was for the SA welds to be made using a matching or over matching filler compared to the parent. These welds were not post-weld heat treated.

4.1.2. Line Pipe Information from Summary Spreadsheet “Linepipe Specs Data v0 [13]”

The line pipe standards reviewed refer to the fact that the product supplied should be consistent with API 5L with additional requirements specified in the applicable British Gas engineering standard. Summary datasheet information was provided from 1968 to 1993. In general, updates followed recommendations from API 5L. Recommendations included updates to composition, in particular the level of carbon, aluminium and total trace elements and for seam welded pipe the need to undertake tensile and sub sized Charpy testing. The following outlines selected information which illustrate how the requirements changed with time:

1. GC PS LX1 May 1968 relates to the supply of submerged-arc welded line pipe manufactured in accordance with the requirements of API Standard 5LX 15th edition in grades up to and including X60. Transverse tensile and impact tests shall be made on this plate and a record maintained of the end from which samples are obtained. The impact tests shall be made at -20 °C and 50 °C (three two-third size Charpy specimens at each temperature).
2. GC PS LX3 Dec 1968 relates to the supply of seamless line pipe of 12 3/4" OD and under manufactured in accordance with the requirements of API Standard 5LX 15th edition in grades up to and including X60. The composition shall conform to API 5LX except that the carbon content shall not exceed 0.24%, the nitrogen content shall not exceed 0.008%, and that the total residual elements shall not exceed 0.8%. The nitrogen content shall apply to open hearth or oxygen processes only. Similar guidance was provided for pipes of larger diameter.
3. GC PS LX1 1971 relates to the supply of submerged-arc welded line pipe manufactured in accordance with the requirements of API Standard 5LX 18th edition in grades up to and including X60. The carbon content shall not exceed 0.22%, total aluminium content shall not exceed 0.05%, nitrogen content shall not exceed 0.008% and the total residual elements shall not exceed 0.8%.
4. GC PS LX3 1971 relates to the supply of seamless line pipe of over 323.8 mm manufactured in accordance with the requirements of API Standard 5LX 18th Edition in Grades up to and including X60. The carbon content shall not exceed 0.24%, the nitrogen content shall not exceed 0.008% and the total residual elements shall not exceed 0.8%.
5. GC PS LX1 1974 relates to the supply of submerged-arc welded line pipe in grades up to and including X70 manufactured in accordance with the requirements of API Standard 5LX, 19th edition. This does not provide limits for specific carbon content. Instead, the following is noted, it is well established that composition, mechanical properties and weldability are all closely related so that the introduction of micro-alloyed and controlled-rolled steels has made it possible to obtain enhanced mechanical properties in steels of lower carbon content.
6. PS LX4 1975 relates to the supply of seamless line pipe 1500 mm up to and including 450 mm nominal pipe size manufactured in accordance with the requirements of API Standard 5LX 19th edition in grades up to and including X60. The carbon content shall not exceed 0.24%, the nitrogen content shall not exceed 0.008% and the total residual elements shall not exceed 0.8%.
7. PS LX4 1976 relates to the supply of seamless line pipe 1500 mm up to and including 450 mm nominal pipe size manufactured in accordance with the requirements of API Standard 5LX 20th edition in grades up to and including X60. The carbon content shall not exceed 0.24%, the nitrogen content shall not exceed 0.008% and the total residual elements shall not exceed 0.8%.

8. BGC PS LX4 1977 relates to the supply of seamless line pipe 150 mm up to and including 450 mm nominal pipe size manufactured in accordance with the requirements of API specification 5L, 20th edition, in grades up to and including X60. The carbon content shall not exceed 0.24% and the total residual elements shall not exceed 0.8%. In the specific instance of nitrogen, the supplier shall demonstrate that this element is adequately fixed and has no deleterious effect on the material properties. In particular, the freedom from strain ageing must be demonstrated.
9. PS LX1 1977 relates to the supply of submerged-arc welded line pipe in grades up to and including X70 manufactured in accordance with the requirements of API Spec 5LX, 21st edition. This does not provide limits for specific carbon content. Instead, the following is noted, it is well established that composition, mechanical properties and weldability are all closely related so that the introduction of micro-alloyed and controlled-rolled steels has made it possible to obtain enhanced mechanical properties in steels of lower carbon content.
10. PS L1 1984 this specifies the requirements for the manufacture of seamless line pipe 40 mm up to and including 10 m nominal size. The line pipe shall be supplied to API L5 Grade B and this standard. The composition is expected to be based on the API L5 carbon manganese steel but the actual ranges for ladle and product analyses shall be agreed with British Gas.
11. PS LX4 1985 relates to the supply of seamless line pipe 150 mm up to and including 450 mm nominal pipe size manufactured in accordance with the requirements of API specification 5L, 20th edition, in grades up to and including X60. The carbon content shall not exceed 0.24% and the total residual elements shall not exceed 0.8%. In the specific instance of nitrogen, the supplier shall demonstrate that this element is adequately fixed and has no deleterious effect on the material properties. In particular, the freedom from strain ageing must be demonstrated.
12. PS LX4 1986 specifies the requirements for the manufacture of seamless pipe 150 mm up to and including 450 mm nominal size. The pipe shall be supplied to API 5L with the additional requirements specified in this engineering standard. It is well established that composition, mechanical properties and weldability are all closely related so that the introduction of micro-alloyed and controlled-rolled steels has made it possible to obtain enhanced mechanical properties in steels of lower carbon content.
13. PS LX4 1987 specifies the requirements for the manufacture of seamless pipe 150 mm up to and including 450 mm nominal size. The pipe shall be supplied to API 5L with the additional requirements specified in this engineering standard. It is well established that composition, mechanical properties and weldability are all closely related so that the introduction of micro-alloyed and controlled-rolled steels has made it possible to obtain enhanced mechanical properties in steels of lower carbon content.
14. PS LX4 December 1988 defines seamless pipe in the range of 150 mm (5.9 in) to 450 mm (17.7 in) nominal sizes. This covers use of pipe up to Grade X60. The composition is expected to be based on carbon manganese steel, but the actual ranges for ladle and product analyses shall be agreed with the purchaser. Requirements for Charpy Impact and drop weight testing are included.
15. PS LX1 May 1989 defines seamless pipe in the range of 150 mm (5.9 in) to 450 mm (17.7 in) nominal sizes. This covers use of pipe from Grade X42 up to and including X60.

16. PS LX1 August 1989. This specification relates to the supply of submerged arc welded line pipe in Grades up to and including X70 manufactured in accordance with the requirements of API Spec 5LX, 21st edition. It is well established that composition, mechanical properties and weldability are all closely related so that the introduction of micro-alloyed and controlled-rolled steels has made it possible to obtain enhanced mechanical properties in steels of lower carbon content.
17. PS LX4 October 1989. This specifies the requirements for the manufacture of seamless pipe 150 mm (5.9 in) to 450 mm (17.7 in) inclusive nominal size. The pipe is supplied to API 5L Grades up to and including X60. The composition is expected to be based on carbon manganese steel, but the actual ranges for ladle and product analyses shall be agreed with the purchaser. Requirements for Charpy impact and drop weight testing are included.
18. BG PS LX4 June 1990 defines the manufacture of seamless pipe in the range of 150 mm (5.9 in) to 450 mm (17.7 in) nominal sizes. This covers the use of pipe grades up to and including X60. For nominal sizes up to a diameter of 300 mm (10.8 in) with thickness below 12.7 mm (0.500 in), Grade X46 is identified. For nominal sizes of diameter 300 mm (10.8 in) with thickness of 12.7 mm (0.500 in) and for nominal diameters of between 400 and 450 mm (15.7 to 17.7 in) with thickness below 15.9 mm (0.625 in), Grade X52 is identified. For nominal diameter of 450 mm (17.7 in) with a thickness of 15.9 mm (0.625 in), Grade X60 is identified. Requirements for Charpy impact and drop weight testing are included.
19. GBE LX1 August 1993. This Gas Business Engineering Technical Specification specifies the requirements for the manufacture of submerged-arc welded pipe 400 mm (15.7 in) to 1400 mm (55.1 in) inclusive nominal size. The steel grades covered are X52, X60 and X65 with the selection linked directly to the specific pipe dimensions. The composition shall be based on carbon manganese steel, but the actual ranges for ladle and product analyses shall be established as part of the manufacturing procedure qualification. Requirements for Charpy impact and drop weight testing are included.

[redacted]

- [redacted]
- [redacted]
- [redacted]
- [redacted]
- [redacted]

These statistics demonstrate that it is not straightforward to assume that all defects in all components can be known from a simple review of the manufacturing standards. Indeed, direct evidence from inspection and sampling of installed components is critical to provide informed perspective on actual quality.

4.2. Commentary on Documents Related to Welds

The earliest information available to be considered was from April 1969. It was apparent that in all cases the standards had been developed based on best practice approaches for the relevant time. As knowledge increased, changes to the standards were approved by the responsible body. In the current document, selected specifications have been considered and commentary provided.

4.2.1. GC/PS/P2 - Draft Standard for Field Welding of Steel Pipelines [14] - The Gas Council, April 1969.

The following provides a commentary on key points

1. The joint shall have a UTS equal to or greater than the parent material.
2. The welding company shall prepare instruction sheets for girth welds, branch connections, anode lugs and other attachments. These sheets must contain:
    a. Material specification and range of thickness
    b. Joint design and preparation
    c. Welding process or processes
    d. Process consumables include make and brand of electrodes and wires
    e. Size of electrodes and wires
    f. Electrical characteristics, current, polarity, travel speed
    g. Welding position and direction of welding
    h. Pre and post weld heat treatment, including method of heating, temperature range and methods of temperature control.
    i. Method of joint alignment
    j. Time lapse between root runs, hot pass and hot fill,
    k. Number of welders,
    l. Mandatory inspection requirements,

The information sheet does not mandate details of the sequence of fill passes, although the list of required information does state “any other relevant information.”

The document further states that all qualification welds shall be made between full pipe lengths and all operations performed in accordance with production line pipe procedures. Moreover, each weld shall be radiographically tested using an x-ray technique. As determined by the employer, magnetic particle and/or ultrasonic inspections may also be undertaken.

It is stipulated that the quality of the weld shall also be determined by destructive testing. In terms of defects, welds will be considered acceptable if the greatest dimension of any gas pores does not exceed 15% of the wall thickness. There shall be no more than six (6) gas pores present on the surface examined. The maximum dimension of the largest slag inclusion shall not exceed 15% of the wall thickness. There shall be no more than ten (10) smaller slag inclusions present on the section examined. The accumulated total of the slag inclusions shall be not more than 30% of the area of the section examined.

Guidance is also provided for post weld bend testing, tensile testing, preparation and examination of macro sections, hardness measurements and Charpy V-notch impact testing. The recommendations state that the hardness of the weld metal shall be greater than that of the parent but not by more than 75 HV. Hardness criteria for the heat affected zone (HAZ) state that for the cap run the hardness shall not be more than 125 HV greater than the parent, whereas for the weld root the maximum hardness in the HAZ shall be not more than 75 HV greater than the parent.

For the Charpy V-notch impact testing, the requirement given is that for testing at 0 °C, the average of three (3) tests shall be at least 27 J (20 ft-lbf) with no individual test having a measured value of less than 20 J (15 ft-lbf).

Repair Welding

Joints which do not meet the defined acceptance criteria shall be repaired. The remediation may involve complete removal of the original weld and rewelding, or a local repair may be acceptable. A specific instruction sheet shall be established for manufacture of the repair. The acceptance testing performed must demonstrate that the repair does not result in unacceptable performance of the original weld.

Single pass weld bead type repairs are not allowed unless validated using the full development and acceptance testing.

4.2.2. GC/PS/P2 - Draft Standard for Field Welding of Steel Pipelines [15] - The Gas Council, December 1970.

This document specifically states that the standard for field welding is based on API 1101, which was then modified based on the research experience and expertise of UK Gas industry. The document format is similar to API 1104 but the content is presented with two main parts dealing with Welding and Inspection. This specification emphasizes the need for complete visual inspection to check aspects of set up and welding, as well as 100% radiographic testing of girth welds. The radiographic inspection can be supplemented by eddy current testing, magnetic particle testing or volumetric examination using ultrasonic testing.

4.2.3 BGC/PS/P2 - Specification for Field Welding of Steel Pipelines and Installations for High Pressure Gas Transmission [16] - British Gas. April 1981.

This is an updated version of previous specifications containing similar information. There are several differences worthy of note. These include:

1. A typical layout for the weld information sheet is provided
2. It is recognized that girth welds can be manufactured between different pipe sections so the hardness rules are changed to indicate that the hardness of the weld should not be greater than 75 HV higher than the harder pipe section.
3. It is acknowledged that the dimensions of the Charpy V-notch samples will depend on the size of the pipe. For pipe of 12 mm (0.472 in) or greater thickness, samples can be the standard size of 10 mm (0.394 in) by 10 mm (0.394 in) and the Charpy energy for tests at 0 °C (32°F) shall be 27 J average with no individual test being less than 20 J (15 ft-lbf). For pipe of nominal wall thickness of 8.0 to 9.5 mm (0.314 to 0.354 in) samples should be 10 x 6.7 mm (3.94 to 0.263 in) and the Charpy energy for tests at 0 °C (32°F) should be 20 J (15 ft-lbf) mean with no individual test being less than 14 J (10 ft-lbf). For pipe of nominal wall thickness of 6 mm (0.236 in) samples should be 10 x 5 mm (0.394 x 0.197 in) and the Charpy energy for tests at 0 °C (32°F) should be 20 J (15 ft-lbf) mean with no individual test being less than 14 J (10 ft-lbf).

4. Acceptance criteria include weld fit up, for pipes of similar dimensions the misalignment shall be less than 1.5 mm (0.059 in).
5. Good alignment shall be achieved using specialist clamps, the use of temporary attachment welds is not permitted.

4.2.4. BGC/PS/P2 - Specification for Welding of Land Pipelines and Installations Designed to Operate Above 7 bar (102 psi) [17] - British Gas. July 1991.

This specification replaces previous documents [15] (1981) and [18] (1985) and was based on information from British Standard 4515:1984 [19]. The specification covers requirements for arc welding and inspection of butt joints, branch connection and fillet welds in carbon, carbon manganese and low allow steel land pipeline and installations. The following welding processes are covered by the specification: manual metal arc, submerged arc, metal inert gas, metal active gas, tungsten inert gas, carbon dioxide and non-shielded welding.

The summaries from the quoted specifications begin with a document published in 1969. No details were available for earlier versions. It is clear that the different documents produced over time involved adding additional detail and requirements. The specifications in themselves do not allow the influences/risks of operation in hydrogen gas to be identified unambiguously. More commentary on these issues has been provided in the sections which follow.

4.3. Commentary on Approaches for Quality Assurance

The methods of quality assurance involved both non-destructive and destructive testing. The individual specifications provide guidance on the required tests and the acceptance requirements. In addition, expert reports are available which provide complimentary information regarding undertaking the required non-destructive inspection and provide additional guidance on interpretation of the data, particularly with respect to identification of porosity, inclusions, incomplete root penetration, lack of root fusion, and identification of cracks (e.g. [20]). These documents also emphasize and provide information regarding safety.

4.3.1. Non-destructive Inspection

As described in [14] (1970), the review of the radiographic testing will be considered in terms of four (4) categories: these are:

a. Category 1. Cracks, cracking will not be allowed. If crater cracks are identified these may be repaired.
b. Category 2. Lack of sidewall fusion or inadequate penetration, incomplete fusion or root undercut are permitted provided the defect length does not exceed 25 mm (1 in) in any 300 mm (1 ft) length
c. Category 3. Slag with a size less than 3 mm (0.125 in) and other non-crack like defects, provided the length does not exceed 50 mm (2 in) in a length of 300 mm (12 in).
d. Category 4. Slag and porosity with a size greater than 3 mm (0.125 in) shall be assessed using acceptance diagrams provided. However, acceptance is dependent on pipe

thickness. Burn through shall not exceed 5 mm and only one region of burn through is permitted in a length of 300 mm (12 in).

In 1970 fracture mechanics methods for engineering decision making were under development. Thus, it is not known how the acceptance criteria were justified.

The details of the non-destructive testing and associated acceptance criteria were reviewed and updated in subsequent standards. The changes generally included additional requirements or details. For example, in [21] (1971) the requirements included 100% radiography of all girth welds and butt weld in attachments. As noted previously, magnetic particle and ultrasonic volumetric examinations could also be performed. The categories for acceptance were similar; however, in Category 2 the acceptable defect length was increased to "not to exceed 50 mm (2 in) in a length of 300 mm (12 in)". Tungsten inclusions were specifically identified as a defect.

In general, there were only minor changes to the stated requirement through standards published to 1988.

4.3.2. Destructive Testing

Destructive testing is a requirement of the weld procedure development. Typically, several types of tests are required, namely:

a. Sectioning and preparation for macroscopic examination
b. Tensile testing
c. Bend testing
d. Hardness testing, and
e. Charpy V-notch testing.

The requirements for these tests are provided in the specification, and full details are given in appropriate reference documents. It should be noted that while in selected engineering applications, data from Charpy tests can be used as an analogue for fracture toughness, the correlations proposed are frequently identified after conducting several series of experiments. This type of empirical link is particularly difficult to achieve when considering performance in hydrogen because the process of Charpy testing is very different to that of a Code recommended fracture toughness test. Thus, Charpy results do not necessarily provide a meaningful guide to fracture behaviour in hydrogen.

4.3.3. Commentary and Evaluation of the Quality of Welds Tested

Methods for the manufacture of welds used in engineering applications are typically developed and qualified using:

- Weld Procedure Specification (WPS) which documents the instructions that govern the fabrication process, and
- Procedure Qualification Record (PQR) which details the results obtained for the mandated tests.

Access to WPS and PQR documentation was provided by NGT and a few examples are shown here to illustrate the issues identified.

It should be noted that the documents available did not cover all vintages of pipe. Moreover, no detail of the WPS or PQR documentation was provided for fabrication of the seam welds. Thus, it is not possible to comment on the risks of hydrogen damage in all vintage circumferential welds nor the seam welds. Post service destructive examinations have allowed insight into potential risk factors; these results were presented in Section 3 and the implications with respect to damage during transmission of hydrogen are discussed later in this document.

An example of less than desirable fit up taken from one of the post weld destructive examination records is shown in Figure 21.

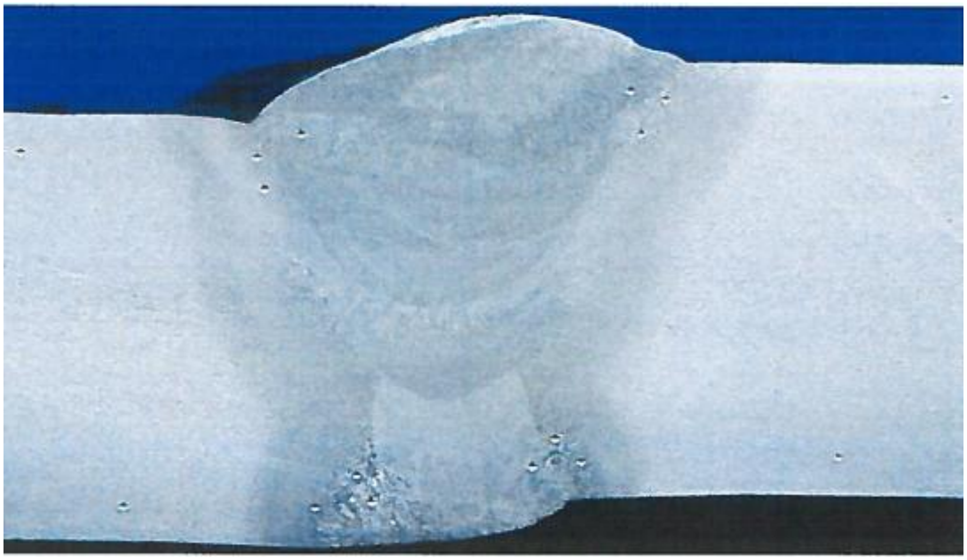

Figure 21. Macrophotograph showing the appearance of weld in report MAN 212568

This macrophotograph shows that the opposite sides of the girth weld had not been properly aligned at fit up prior to welding. Poor fit up introduces local stress concentrations which can influence in-service performance. Moreover, the variation will influence local heat flow. The image in Figure 21 also shows the locations where hardness tests were made. Most of the readings were taken in the weld metal and HAZ at the weld root.

The measured hardness values for welds made in similar base steels show variations, both from weld to weld and in values taken from different locations in the same weld. For example, data from WPQR-B118 showed hardness values in the range from 249 and 351 HV10 in the HAZ at the inner diameter (ID) and 277 to 306 HV10 in the weld at the ID. These values may be considered reasonable for the natural gas service which is what these pipes were designed and fabricated for; however, current thinking is that hardness values over 275 HV in line pipe exhibit an increased risk of hydrogen embrittlement and therefore are not recommended hydrogen service [8]. Note that this is an increase from the 250 HV value cited in ASME B31.12 (2023) [3].

Examples of Charpy V-notch values in the brittle regime were recorded. However, even for sub sized specimens tested at 0 °C, values of 14 J (10 ft-lbf) are considered acceptable in the specification.

4.3.4. Discussion and Concluding Comments

Analysis and additional testing have been carried out to investigate some of the concerns raised here and the reports produced were reviewed. For example, reference [22] details analysis to assess the risk of fast fracture in pipes with low Charpy V-notch values which were part of the NTS.

Charpy V-notch does not provide a direct measure of fracture toughness; however, it has been used extensively as a metric for qualifying line pipe because it is inexpensive, convenient and widely available. From a geometry and loading condition perspective, Charpy testing is performed on a small specimen with a rounded notch that is subjected to extremely high strain rates, with the resulting output being a combination of the energy required to initiate and propagate the crack. On the other hand, fractures toughness tests are conducted on specimens with very sharp cracks that are loaded at strain rates several orders of magnitude slower than an impact test. As such, while Charpy testing in air may help to identify material that may have inherent brittleness, there is no indication that such testing will provide meaningful data to assess how a pipeline steel will perform in hydrogen service.

In other work, [20] post service evaluation of 36 ex-service samples from a number of pipelines of which 26 samples contained defects is described. All samples were taken from ex-service pipes which had not failed, even during hydrotesting. Of the 26 defective welds there were examples of cracks, porosity, undercut, lack of fusion, excess penetration and other defects. It was reported that the tendency for defective welds was similar in vintage and modern pipes [20]. None of the samples examined showed hardness values above 250 HV. A program of fatigue endurance testing showed that the BS 7608 [23] F2 design curve could be used to model the fatigue behaviour of vintage samples containing defects [21].

4.3.5. Summary

Experience shows that even when there are defects present in pipeline girth welds, failures are relatively uncommon. However, good serviceability has been achieved by the fact that

- The design is relatively conservative,
- The level of fatigue loading is low, and
- The steels used typically exhibit reasonable fracture resistance.

The fact that components in the NTS have shown hardness values which have been identified as ‘of concern’ in hydrogen applications is an issue which should be further evaluated. The influence of the high hardness should be considered further because laboratory testing has identified a relationship between hardness and the susceptibility to hydrogen embrittlement. It should also be noted that for welds the highest hardness values were not necessarily measured at the outside or inside surfaces. Recent work studying the influence of defects on performance in hydrogen is discussed later.

5. Post-test Characterisation of Weld Fracture Toughness Specimens (WP2)

Over the past decade, EPRI’s materials group has standardized procedures and methods to properly pedigree materials, characterize microstructure, and assess damage in structural components. EPRI’s approach to characterizing materials includes performing analyses at three different length scales: macro-, micro-, and nano- scale. The results of metallographic assessment (by EPRI and collaborators) on the base metal, heat affected zones and weld metal (seam and girth) of the specific line pipe steels of interest was reported in Section 3 of this report. The experimental work in this section focuses on post test assessment of the fracture toughness (FT) specimens.

EPRI evaluated ex-service line pipe samples from the NTS that were tested in hydrogen by an experienced third-party contractor. An outline of the experimental procedure used by the contractor and provided to National Gas for the FT testing is provided, followed by details of the post test characterization methods and results.

5.1. Fracture Toughness Testing in Hydrogen

Fracture testing was performed using compact tension (CT) specimens that were extracted from the base metals and girth welds in the L-C orientation such that the through-thickness notch was in the circumferential direction. For seam welds, the CT specimens were oriented in the C-L orientation with the through-thickness notch in the longitudinal direction. Test specimens were removed from the middle of the pipe wall and machined to a thickness of 12.7 mm (0.5 in) and width (W) of 25.4 mm (1.0 in). For weld samples, the notches were placed either at the weld centreline (WCL) or in the heat affected zone (HAZ) approximately 1.0 mm (0.039 in) from the weld fusion line at the mid-thickness. Grooves were machined into the sides of all test specimens to reduce the thickness and help keep the crack in plane during testing; side grooves extended approximately 5% into each side of the test specimen. Prior to testing, the specimens were pre-cracked in air via fatigue to achieve an initial crack depth ratio (*a/W)* of ~0.50, where '*a*' is the length of crack.

Hydrogen testing was carried out in high pressure autoclaves. Samples were loaded into the loading cage and pressurized with high purity nitrogen to ensure the system was leak-tight, then depressurized. The system was subsequently repressurized with nitrogen gas and purged three more times to minimize the oxygen and moisture content in the system. Hydrogen was flowed through the system until the oxygen concentration on the gas analyser was below 1 ppm. The autoclave was then pressurized with pure hydrogen to 69 bar (1000 psig) and pre-soaked for five hours prior to loading the specimen.

Fracture testing was performed in accordance with ASTM E1820 [24] using a rising displacement test method and direct current potential drop (DCPD) for crack monitoring. Tests were conducted a using a constant displacement rate corresponding to a loading rate (dK/dt) of ~0.5 MPa√m/h (0.45 ksi√in/h) . Upon completion of the test, specimens were removed from the autoclave and heat tinted to highlight the final crack path in hydrogen gas.

Analysis was performed to calculate the variation in *J* as a function of crack extension (D*a*), which is expressed as a J-R curve. From the J-R curve, the fracture resistance values at crack initiation (J_{0-H}) and at the 0.2 mm construction line ($J_{0.2-H}$) were obtained. Recorded values of *J* were then converted to *K* at specific crack extensions (i.e. 0.0 mm and 0.2 mm) through the relationship provided in ASTM E1820 [24]:

$$K_J = \sqrt{\frac{\mathrm{E}}{(1-\upsilon^2)}J}$$

where E is Young's modulus (assumed to be 200 GPa), ν is Poisson's ratio (assumed to be 0.3) and *J* is measured in N/mm.

5.2. Characterization Procedures

Post test assessment of the fracture surfaces was carried out using an approach designed to link the physical evidence present on the fracture surfaces with the recorded fracture resistance values. The fracture surfaces were initially analysed using a Keyence VHX-7000 digital optical microscope to produce a three-dimensional (3D) optical image of each fracture face at 50× magnification. The data from these images were analysed within the first one millimetre of crack extension into the hydrogen test region (i.e., from the end of the fatigue pre-crack to Δa = 1.0 mm [0.039 in]). To properly visualize the planarity of the fracture surface, the raw 3D data from the optical image was extracted using the Keyence software, then converted to standard Z-height map and sliced at 0.1 mm (0.004 in) intervals to collect individual profile lines. Over 35 million datapoints were extracted from each sample with an X and Y resolution of 0.002 mm.

5.3. Results

A particular goal of the post-test examination was to document features associated with the transition from the fatigue pre-crack to the region where fracture toughness was assessed. As noted, this process involved making 3D optical scans using the Keyence VHX-7000 digital optical microscope. As shown schematically in Figure 22A, in the current work, data from the nominally 6 mm (0.236 in) thickness of the CT samples were plotted over a distance of 2.0 mm (0.079 in). Three-dimensional (3D) optical stitched images of each fracture face were captured at 50× magnification, and a two-dimensional (2D) representation of the fracture face was used for evaluating each zone of the test specimens and as a method to document initial observations.

Results from the base metal test on sample X60A are presented initially. The base metal sample was selected as it provided the least heterogeneous of the specimens tested. The photograph of the fracture surface presented in Figure 22B shows several noteworthy features. Firstly, cracking has developed perpendicular to the direction of the machined notch and subsequent fatigue pre-crack (FPC). This damage is consistent with the presence of inclusion stringers in the steel. Secondly, it is apparent that within the first 1.0 to 2.0 mm (0.039 to 0.079 in) of crack growth, the crack front is non-uniform. This is evidence of variability of the crack development in hydrogen, Figure 22B.

Further, evidence of the complexity associated with the crack growth in hydrogen is revealed from the 3D scans. The images presented in Figure 22C and 22D indicate that there are changes in the plane of crack growth. Of particular interest, is the fact that the results suggest that even within the first 1.0 mm (0.039 in) of growth from the fatigue pre-crack, there are significant deviations from the expected plane of cracking. These complexities are consistent with the fact that local constituents and microstructure influence the performance in hydrogen.

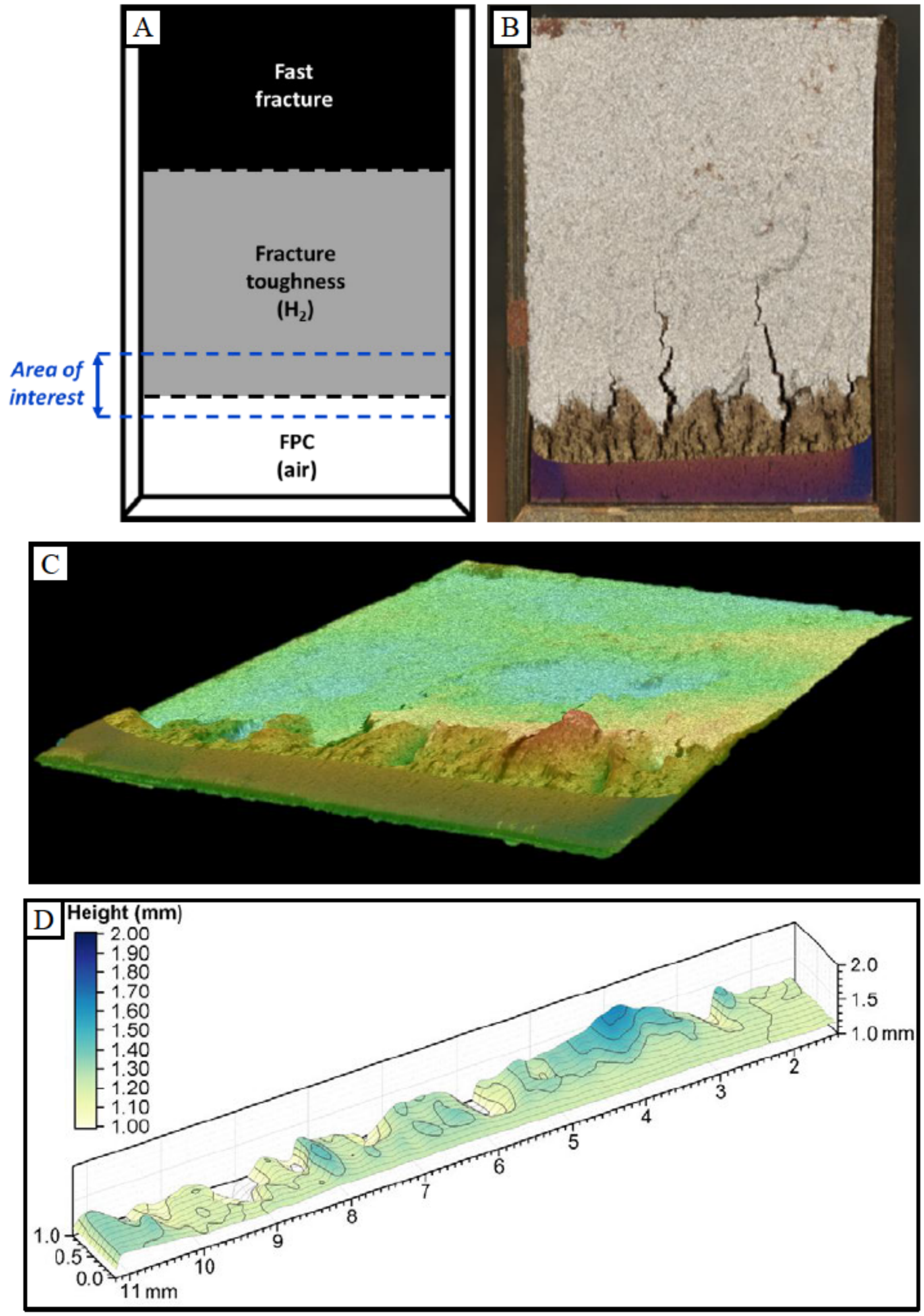

Figure 22. (A) schematic diagram showing the different zones on the fracture surface highlighting the area of interest for detailed mapping; (B) representative fracture surface for base metal X60A after testing in hydrogen; (C) 3D reconstruction of the fracture surface shown in (B); (D) 3D plot showing the fracture features within the area of interest indicated in (A)

A photograph of the fracture surface of the X60A GWHAZ specimen tested in hydrogen is presented in Figure 23. The appearance of the fracture surface shows that cracking which was approximately perpendicular to the expected plane of crack growth had developed. Furthermore, the growth of the crack front is non-uniform, with variations in the crack extension (Δa) during in-hydrogen testing being between <1 mm and 4.3 mm (<0.039 and 0.169 in).

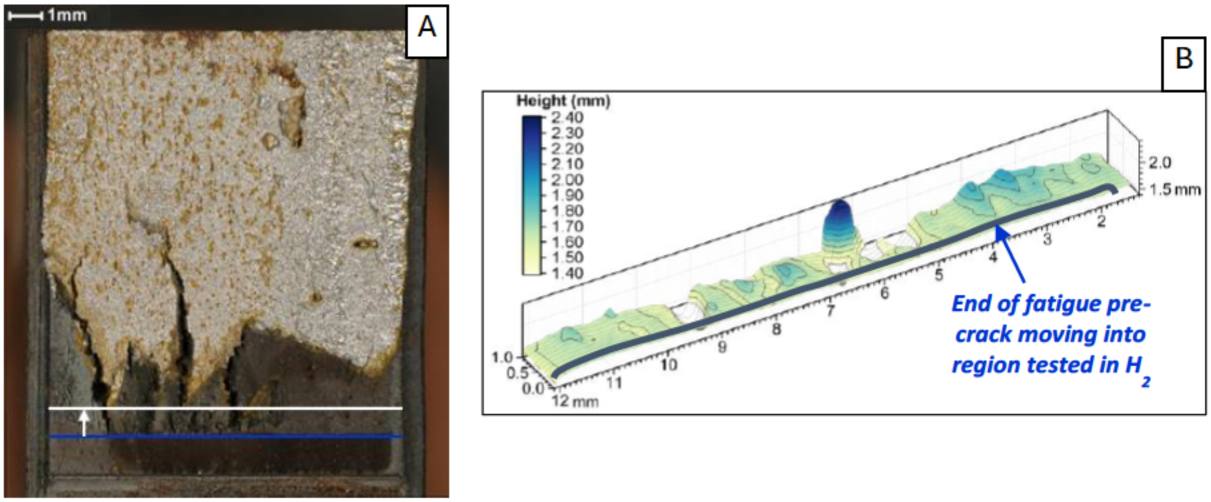

Figure 23. (A) Photograph of the fracture surface of X60A GWHAZ, and (B) a detailed 3D plot generated from data collected between the blue and white lines.

As shown in Figure 24, the plane of crack growth in hydrogen of X60A GWHAZ involved several significantly different features. These included:

1. A region of the weld metal which in this plane extended over about 20% of the section,
2. Several anomalies, most likely linked to inclusions, were perpendicular to the expected plane of cracking. In several cases these anomalies had opened to form cracks.
3. Variability in the microstructure of the HAZ. It is not apparent how much of the HAZ adjacent to the fusion line was included in the cracking. This is particularly pertinent as the HAZ nearest the fusion line was shown to exhibit the highest hardness
4. The diversity of features identified appear to have influenced the specific depths of crack growth during testing in hydrogen. This variability must complicate interpretation of the crack growth behaviour and the ability to fully define the response of the DCPD data in terms of meaningful values for fracture resistance.

The appearance of the fracture surface of the X80 girth weld is shown in Figure 25. The extent of the crack front from the pre-fatigue crack is variable. It is apparent that even within the first 0.2 mm of growth there is a shift in the plane of cracking. It appears that the cracking behaviour at about 3 mm of growth is influenced by the existence of a significant defect. It appears that this defect may have influenced both the extent of crack growth and the plane on which the cracking was taking place.

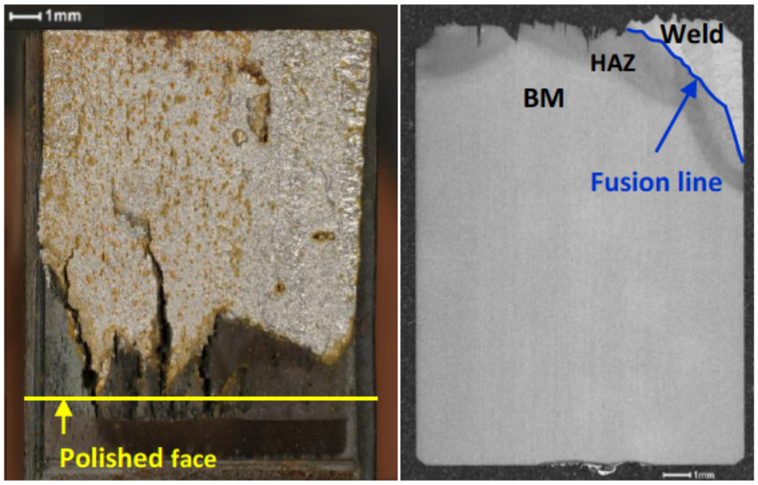

Figure 24. Fracture surface of X60A GWHAZ showing where metallographic sectioning was performed and the etched micrograph showing the microstructural regions intersected by the cracking

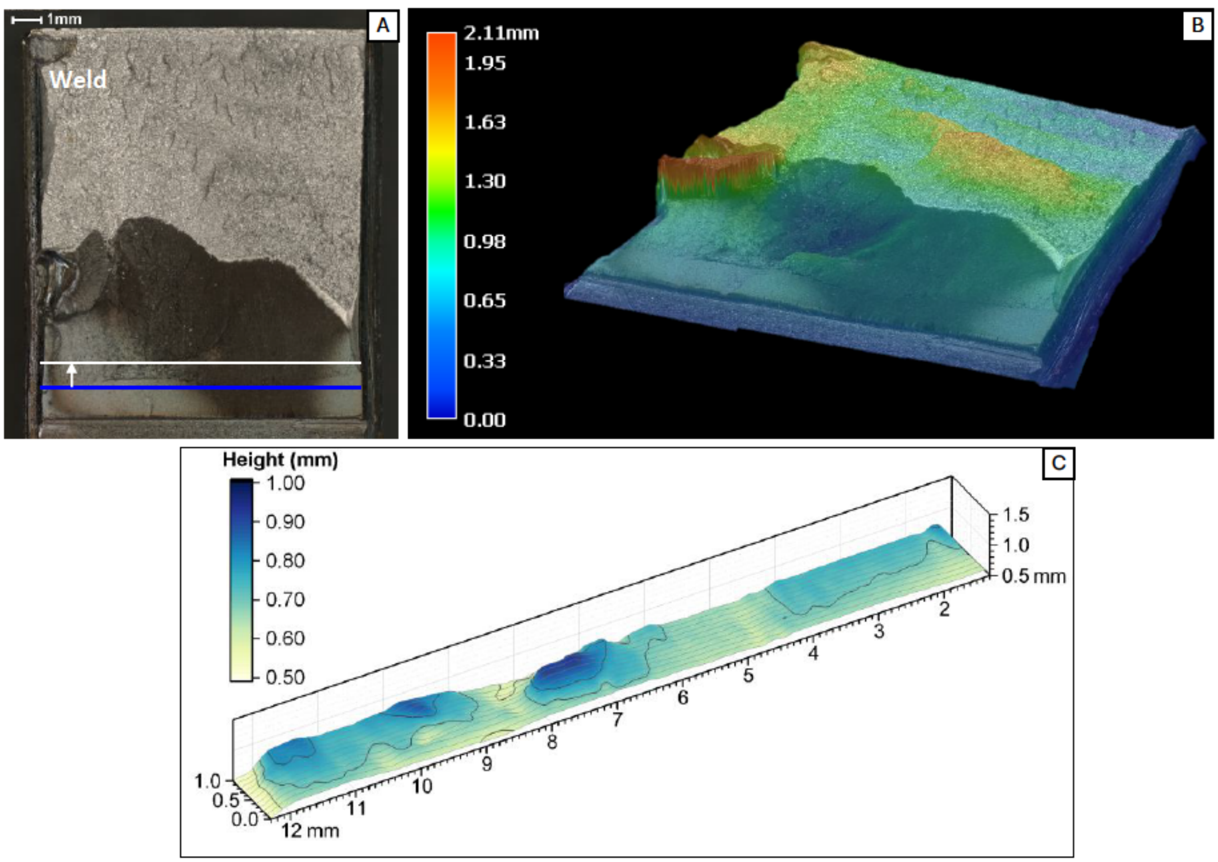

Figure 25. (A) Photograph of the fracture surface of X80 GWHAZ, with 3D topographical maps from the sample surface (B, C)

6. Analysis of Fracture Toughness Data

Fracture toughness testing was performed on single specimens removed from the base metal, seam weld centre line (SWCL), girth weld centreline (GWCL), through thickness samples in the vicinity of the seam weld HAZ (SWHAZ) and a region corresponding to the girth weld heat affected zone (GWHAZ). Test results from the following steels were prioritized by NTS for evaluation as follows:

- X60, 1971 [X60A]: Seam weld heat affected zone (SWHAZ), girth weld heat affected zone (GWHAZ) and base metal (BM),
- X52, 1970: SW HAZ and GW HAZ
- X80, 2007 (2022) [X80]: SWHAZ and GWHAZ,
- X46, 1964: GWHAZ
- X65, 1988: GWHAZ.

Analysis of the test data and fracture surfaces was the basis for commentary and discussion regarding the reported fracture toughness values obtained for compact-tension (CT) samples in hydrogen gas. Effort was focused on samples removed from the heat affected zones of seam and girth welds because data from these tests typically involve variability of microstructures. EPRI was not involved in any aspect of the program of in-hydrogen testing therefore we cannot comment on the testing conditions selected (i.e., test pressure, *K*-rate, oxygen content, moisture content, testing apparatus, etc.). However, the laboratory undertaking the testing was experienced in testing of this type and it is understood that hydrogen had sufficient time to diffuse into the steel and to the crack tip before and during loading. The analysis and commentary on the testing results, is primarily based on:

- Post test characterizations and analysis of the fracture surface (described in Section 5).
- Knowledge of sample geometry.
- Review of the J-R curves and Load vs. Crack Mouth Opening Displacement (CMOD) curves provided by NTS.
- The latest understanding (from hydrogen testing experts) on how the findings can and should be used to make informed decisions regarding integrity management of pressure containing components in gaseous H_2 service.
- It is emphasized that this field is still the subject of active research with ongoing developments.

In Table 2, the average (Δa_{Avg}) and maximum (Δa_{Max}) crack extension by direct measurement were compared with DCPD (Δa_{DCPD}) values during testing. Percent error was calculated as ($\Delta a_{DCPD} - \Delta a_{Avg}$)/$\Delta a_{DCPD}$, and in all but one case, the error would be above 20% if Δa_{Max} was used. For this evaluation, only data from the first 1.0 mm of crack extension was considered, which spans the applicable range for fracture toughness assessment.

Table 2. Comparison of crack extension values measured using the DCPD instrumentation during in - H_2 testing with post test laboratory measurements. Note, % Error was calculated as $(\Delta a_{DCPD} - \Delta a_{Avg})/\Delta a_{DCPD}$.

Test ID	Grade	Year	Sample ID	Δa_{DCPD} (mm)	Δa_{Avg} (mm)	Δa_{Max} (mm)	%Error
4859	X60	1971	SW HAZ-1	11.485	11.322	12.457	1.4
			GW HAZ-1	2.826	2.353	4.467	16.8
4621	X52	1970	SW-HAZ-1	2.171	2.092	3.667	3.6
			SW HAZ-3	7.817	8.961	10.270	-14.6
			GW HAZ-1	1.612	1.520	2.086	5.7
4862	X80	2000	SW HAZ-1	6.558	6.298	8.069	4.0
			GW HAZ-1	4.686	4.296	5.789	8.3
4834	X46	1964	GW HAZ-2	2.083	2.350	3.492	-12.9
			GW HAZ-3	2.179	2.206	3.438	-1.2
4861	X65	1988	GW HAZ-1	2.135	2.072	3.480	2.9

The unique identification number was assigned to each data set (Test ID) and specific sample designations within the data set (Sample ID) by the third-party testing laboratory. For the analysis and presentation of the layout, the formatting for each plot type (J-R or Load versus CMOD) is consistent for ease of comparison between data sets.

This comparison involves the following information:

- *J*-integral (y-axis) ranges from 0 to 100 N/mm
- Δa (x-axis) ranges from 0 to 1.0 mm
- Base metal curves are green triangles
- Girth weld curves are black/grey squares
    - WCL closed black
    - HAZ open grey
- Seam weld curves are blue circles
    - WCL closed dark blue
    - HAZ open light blue

The results of the data review and analysis are presented for specific grades and vintages in the following sections.

6.1. Results for Tests on Samples from X60A

The J-R fracture resistance curves for sample X60A are shown in Figure 26.

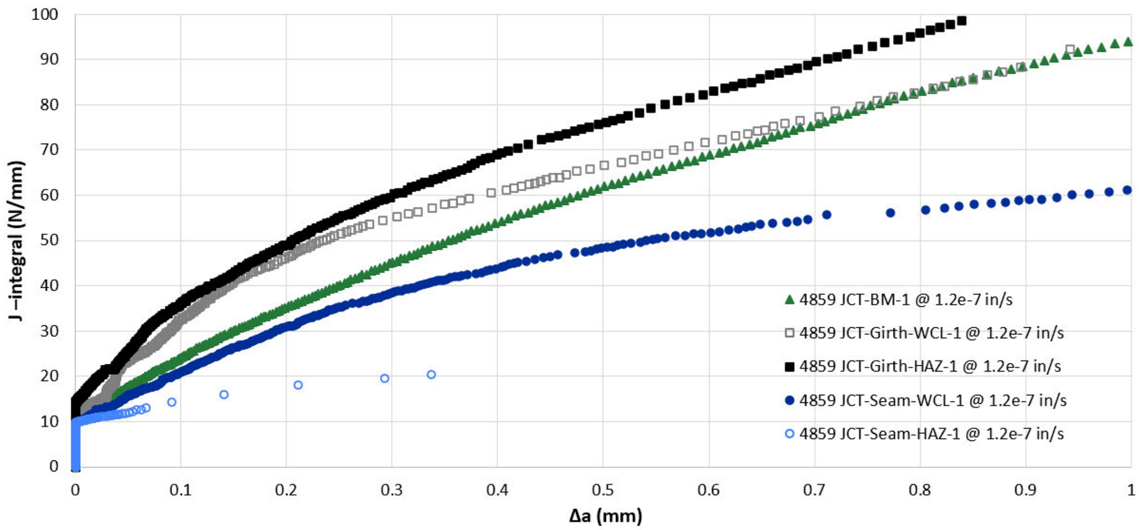

Figure 26. J-R curves for X60A specimens removed from the base metal, GWCL, GWHAZ, SWCL and SWHAZ. Shown here are results from only one CT specimen at each location.

The relationships between Load and Crack Mouth Opening Displacement are presented in Figure 27.

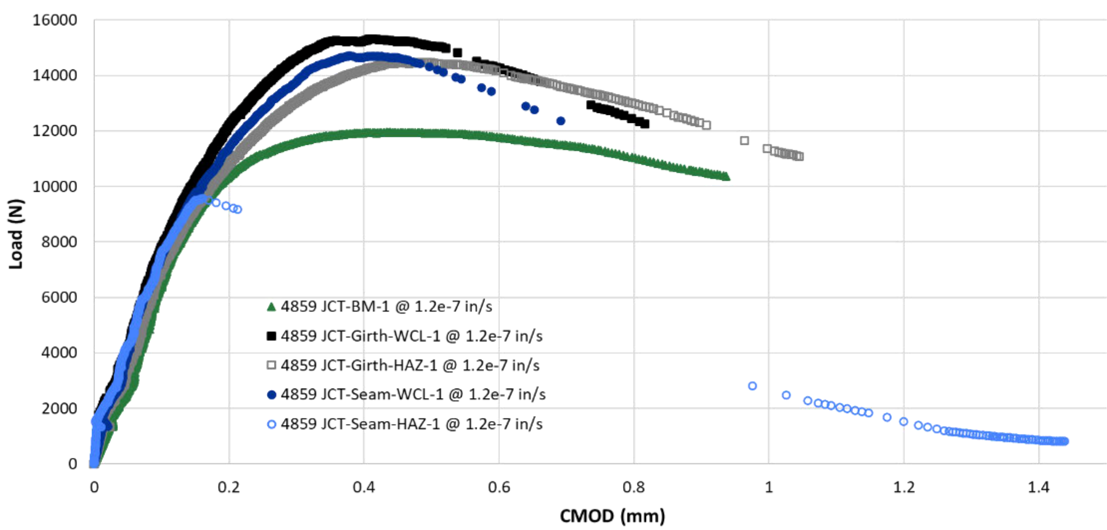

Figure 27. Load versus CMOD for X60A specimens removed from the base metal, GWCL, GWHAZ, SWCL and SWHAZ locations.

From these J-R curves, fracture toughness at crack initiation ($K_{J0\text{-}H}$) and at 0.2 mm ($K_{J0.2\text{-}H}$) were calculated and the results are presented in Table 3.

Table 3: Comparison of Fracture Toughness and stress intensity values from selected points on the testing curves for samples from X60A.

Sample ID	Sample Location	$J_{0.0mm}$ (N/mm)	$J_{0.2mm}$ (N/mm)	$J_{Max\ load}$ (N/mm)	K_{J0-H} (MPa√m)	$K_{J0.2-H}$ (MPa√m)	$K_{JMax\ Load-H}$ (MPa√m)
BM-1	Base metal	10.0	35.4	58.5	47.2	88.8	114.2
GWCL-1	Girth weld – WCL	12.0	46.4	65.7	51.7	101.6	121.0
GHAZ-1	Girth weld – HAZ	14.3	49.1	77.6	56.4	104.5	131.4
SWCL-1	Seam weld – WCL	9.7	31.1	54.7	46.6	83.2	110.3
SHAZ-1	Seam weld – HAZ	9.9	18.0	13.0	46.9	63.4	53.7

Images of the post test fracture surfaces and metallographic cross sections are shown in Figure 28. These images document that for both the GWHAZ and the SWHAZ the cracking has propagated through several different microstructures. It is also interesting that in SWHAZ it is clear that the crack path has deviated away from the plane which included the slide grooves.

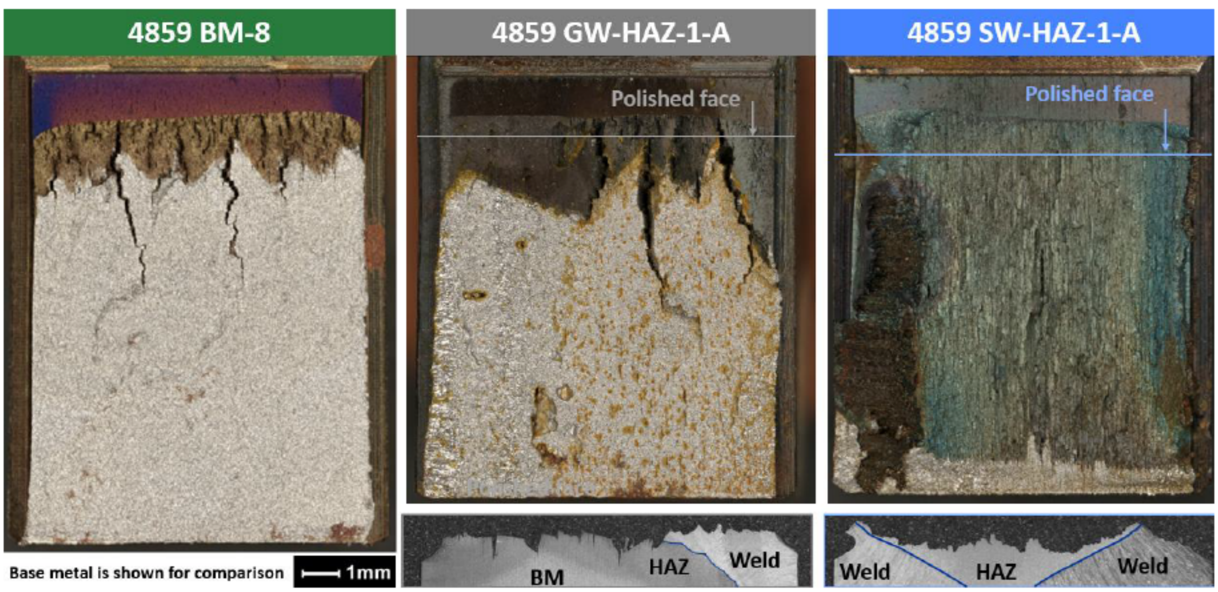

Figure 28. Post test fracture surfaces of base metal, GWHAZ and SWHAZ specimens from X60A. Etched cross sections showing the different HAZ microstructures that the fracture progressed through during gaseous hydrogen testing are illustrated for GWHAZ and SWHAZ.

Analysis of the J-R curves, Load vs. CMOD and post test assessment of the fracture surfaces suggest the following:

- BM-1, GWCL-1 and GW-HAZ-1 all had non-uniform (irregular) crack fronts
- SWCL-1 and SW-HAZ-1 had very uniform cracks fronts that extended almost the full-length of the samples (i.e., nearly broken in half during testing)

- Metallography of the GW-HAZ-1 and SW-HAZ-1 indicated that cracking progressed through portions of the weld metal as well as a variety of HAZ microstructures
  - Significant secondary cracking was noted in the BM-1 and GW-HAZ-1; BM-1 also showed evidence of lamination cracks
- All measured $K_{J0\text{-}H}$ values were relatively similar (46.6 and 56.4 MPa√m), regardless of the type of specimen; however, slopes of the J-R curves were highly variable;
  - GWCL-1 and GW-HAZ-1. Exhibited Steep slope resulting in $K_{J0.2\text{-}H}$ values >100 MPa√m, indicating a high fracture resistance.
  - SW HAZ-1. Exhibited a shallow slope with a measured $K_{J0.2\text{-}H}$ value of 63.4 MPa√m, indicating a low tearing resistance. The $K_{JMax\ Load\text{-}H}$ was 53.7 MPa√m and occurred at Δa = 0.06 mm, suggesting the material was very brittle in hydrogen gas. The peak load was comparatively much lower than the other specimens in the data set.

6.2. Results for Tests on Samples from X52 1970

The J-R fracture resistance curves for sample X52 1970 are shown in Figure 29 with the Load CMOD curves presented in Figure 30.

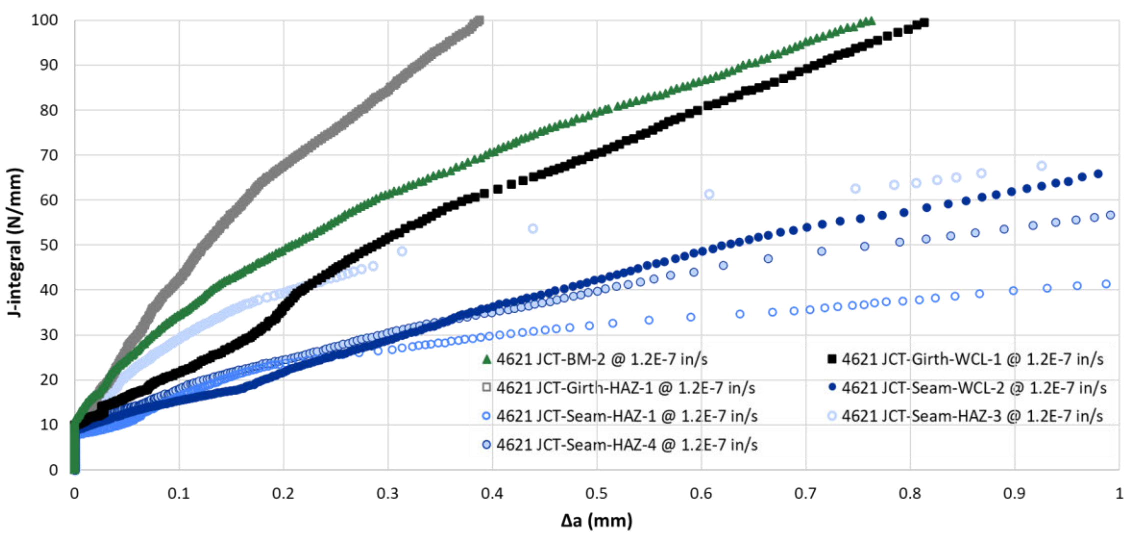

Figure 29. J-R curves for X52, 1970 specimens removed from the base metal, GWCL, GWHAZ, SWCL and SWHAZ. Shown here are results from only one CT specimen at each location.

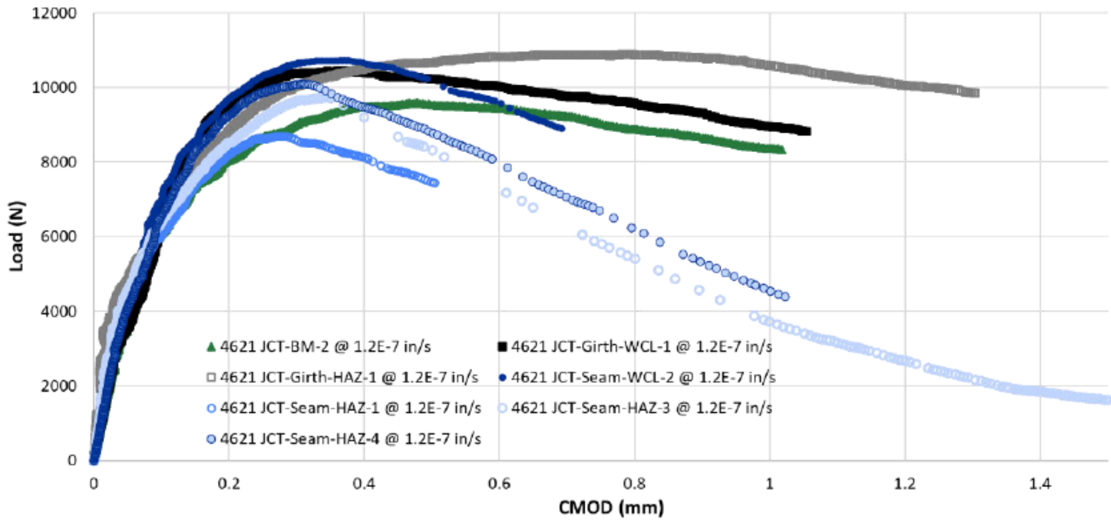

Figure 30. Load versus CMOD for X52 specimens removed from the base metal, GWCL, GWHAZ, SWCL and SWHAZ locations.

Table 4. Comparison of Fracture Toughness and stress intensity values from selected points on the testing curves for samples from X52

Sample ID	Sample Location	$J_{0.0mm}$ (N/mm)	$J_{0.2mm}$ (N/mm)	$J_{Max\ load}$ (N/mm)	$K_{J0\text{-}H}$ (MPa√m)	$K_{J0.2\text{-}H}$ (MPa√m)	$K_{JMax\ Load\text{-}H}$ (MPa√m)
BM-1	Base metal	10.0	35.4	58.5	47.2	88.8	114.2
GWCL-1	Girth weld – WCL	12.0	46.4	65.7	51.7	101.6	121.0
GHAZ-1	Girth weld – HAZ	14.3	49.1	77.6	56.4	104.5	131.4
SWCL-1	Seam weld – WCL	9.7	31.1	54.7	46.6	83.2	110.3
SHAZ-1	Seam weld – HAZ	9.9	18.0	13.0	46.9	63.4	53.7

Post test fracture surfaces and metallographic cross sections from the GWHAZ, SWCL, and SWHAZ of X52, 1970 are shown in Figure 31. As noted, the cross sections for GWHAZ and the SWHAZ show cracking had propagated through several different microstructures, including the base metal, weld metal and heat affected zones. Analysis of the J-R curves, Load vs. CMOD and post test assessment of the fracture surfaces suggest the following:

- All X52 1970 samples exhibited non-uniform (irregular) crack fronts, with most showing some degree of tunnelling (greater extension at the mid-thickness than along the edges).
- Metallography GW-HAZ-1 and SW-HAZ-3 indicated that cracking progressed through a myriad of HAZ microstructures as well as weld metal (~30%) and base metal (~10%) in SW-HAZ-3
    - Secondary cracking was noted in the BM-2 and GW-HAZ-1. In GW-HAZ-1, the cracks were straight and confined to the base metal and HAZ (i.e. not in the weld metal)

- Measured K_{J0-H} values ranged from 41.3 and 49.1 MPa√m, regardless of the type of specimen, Table 4. Slopes of the J-R curves were highly variable:
  - BM-2 and GW-HAZ-1 had relatively steep slopes (to Δa = 0.2 mm), resulting in $K_{J0.2-H}$ values >100 MPa√m
  - Although all SWHAZ samples had similar slopes beyond Δa = 0.2 mm crack extension (suggesting similar resistance to crack propagation, the initial slope of SW-HAZ-3 was considerably higher, resulting in a higher $K_{J0.2-H}$ value (i.e. 93.8 MPa√m as opposed to ~73 MPa√m for SW-HAZ-1 and SW-HAZ-4)
  - The differences in measured toughness between the SWHAZ samples suggest that the microstructural constituents within the HAZ are influencing the crack propagation behaviour in gaseous hydrogen.

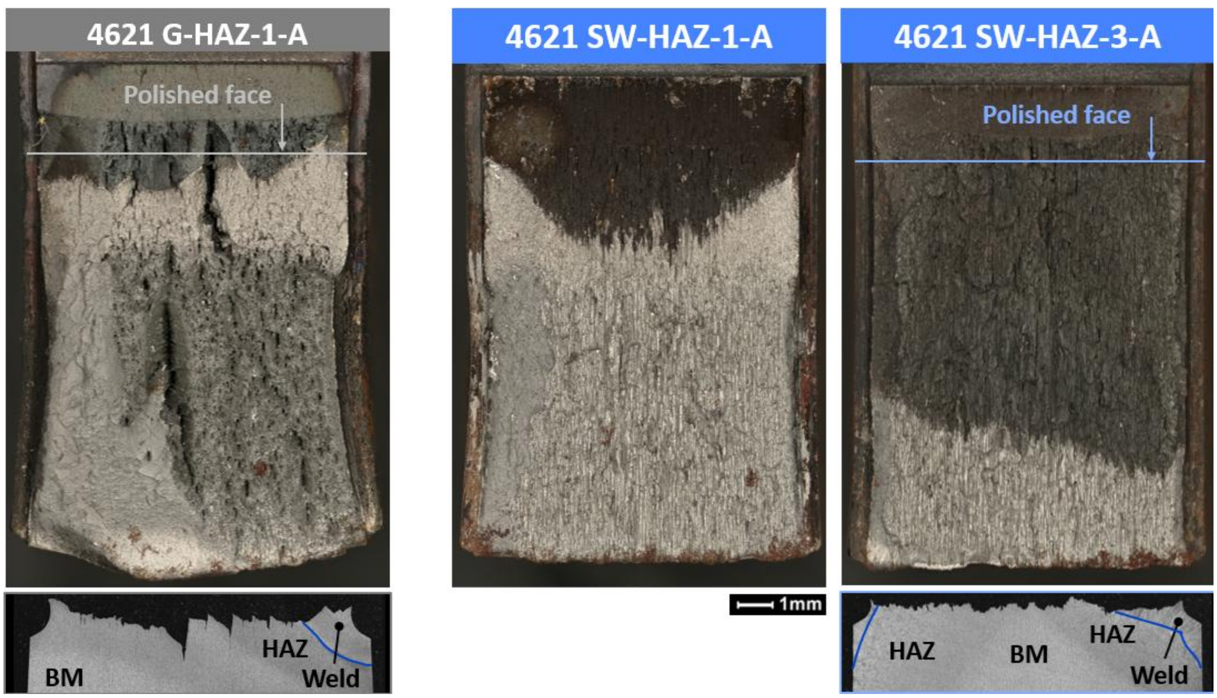

Figure 31. Post test fracture surfaces of base metal, GWHAZ and SWHAZ specimens from X52. Etched cross sections showing the different HAZ microstructures that the fracture progressed through during gaseous hydrogen testing are illustrated for GWHAZ and SWHAZ.

6.3. Results for Tests on Samples from X80, 2007 (2022)

The J-R fracture resistance curves for sample X80 2007 (2022) are shown in Figure 32 with the Load CMOD curves presented in Figure 33.

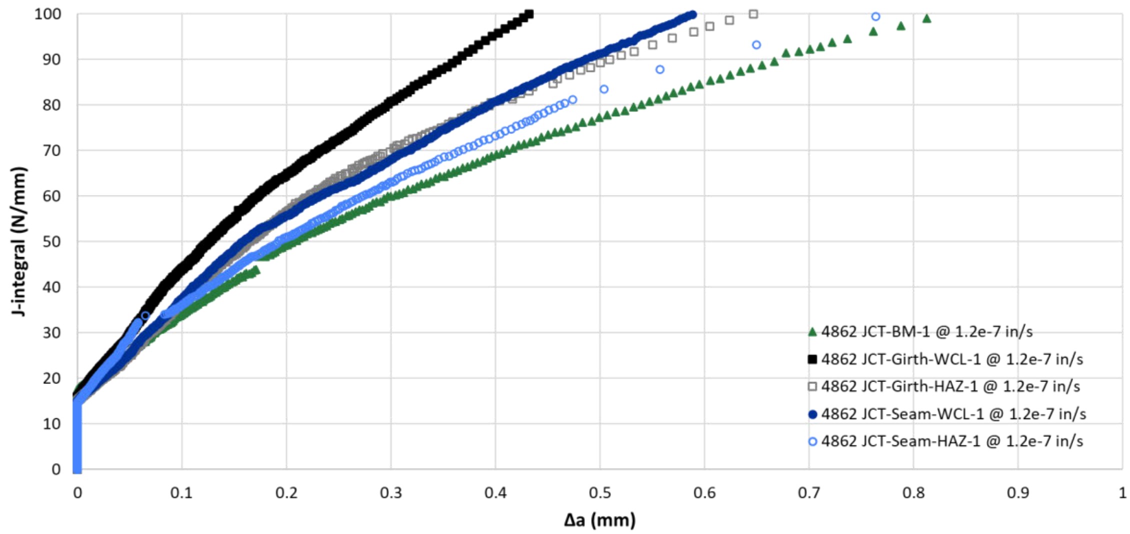

Figure 32. J-R curves for X80 2007 (2022) specimens removed from the base metal, GWCL, GWHAZ, SWCL and SWHAZ. Shown here are results from only one CT specimen at each location.

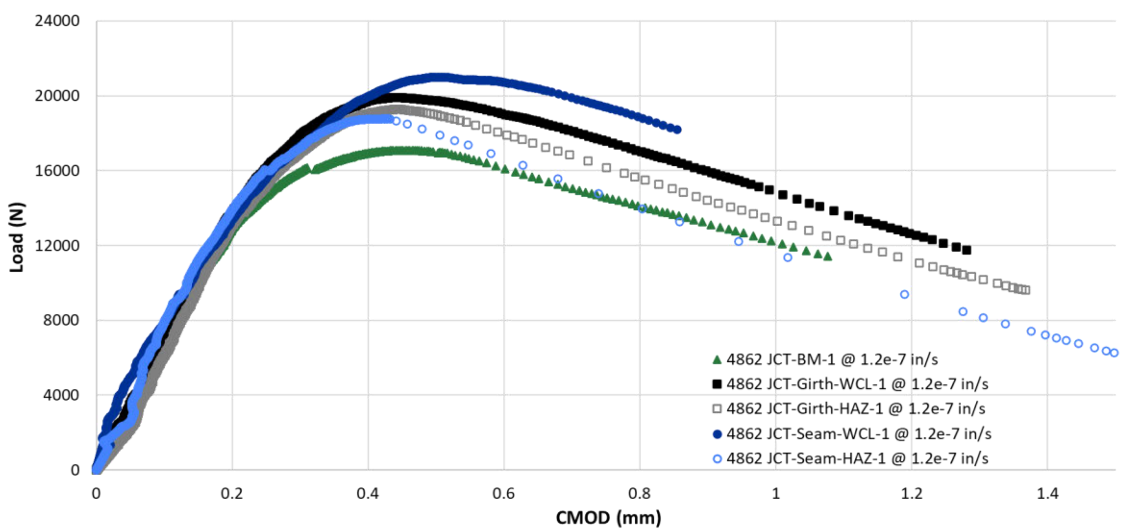

Figure 33. Load versus CMOD for X80 specimens removed from the base metal, GWCL, GWHAZ, SWCL and SWHAZ locations.

Table 5. Comparison of Fracture Toughness and stress intensity values from selected points on the testing curves for samples from X80.

Sample ID	Sample Location	$J_{0.0mm}$ (N/mm)	$J_{0.2mm}$ (N/mm)	$J_{Max\ load}$ (N/mm)	$K_{J0\text{-}H}$ (MPa√m)	$K_{J0.2\text{-}H}$ (MPa√m)	$K_{JMax\ Load\text{-}H}$ (MPa√m)
BM-1	Base metal	17.6	49.2	79.5	62.5	104.7	133.1
GWCL-1	Girth weld – WCL	15.8	64.9	84.1	59.3	120.2	136.9
GHAZ-1	Girth weld – HAZ	15.1	56.8	81.4	58.0	112.5	134.6
SWCL-1	Seam weld – WCL	15.0	55.8	102.5	57.9	111.5	151.1
SHAZ	Seam weld - HAZ	14.6	51.1	80.4	57.0	106.7	133.8

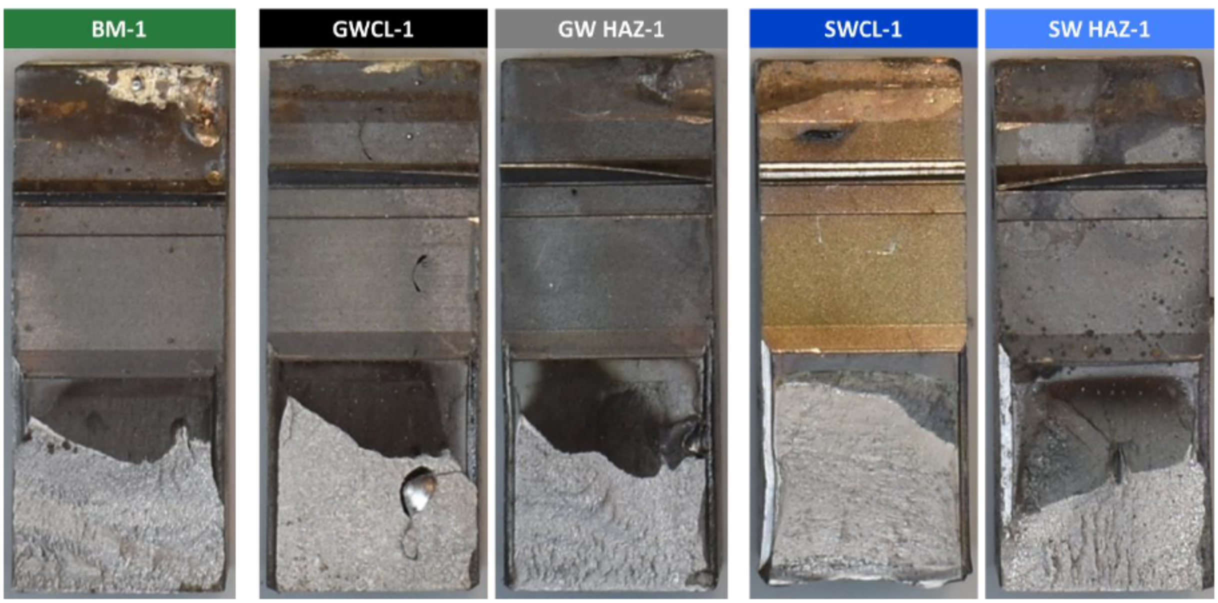

Figure 34. Post test fracture surfaces of base metal, GWHAZ and SWHAZ specimens from X80.

Analysis of the J-R curves, Load vs. CMOD and post test assessment of the fracture surfaces suggest the following:

- [redacted]
- [redacted]
- [redacted]
  - [redacted]

[redacted]

6.4. Results for Tests on Samples from X46, 1964

The J-R fracture resistance curves for sample X46 are shown in Figure 35 with the Load CMOD curves presented in Figure 36.

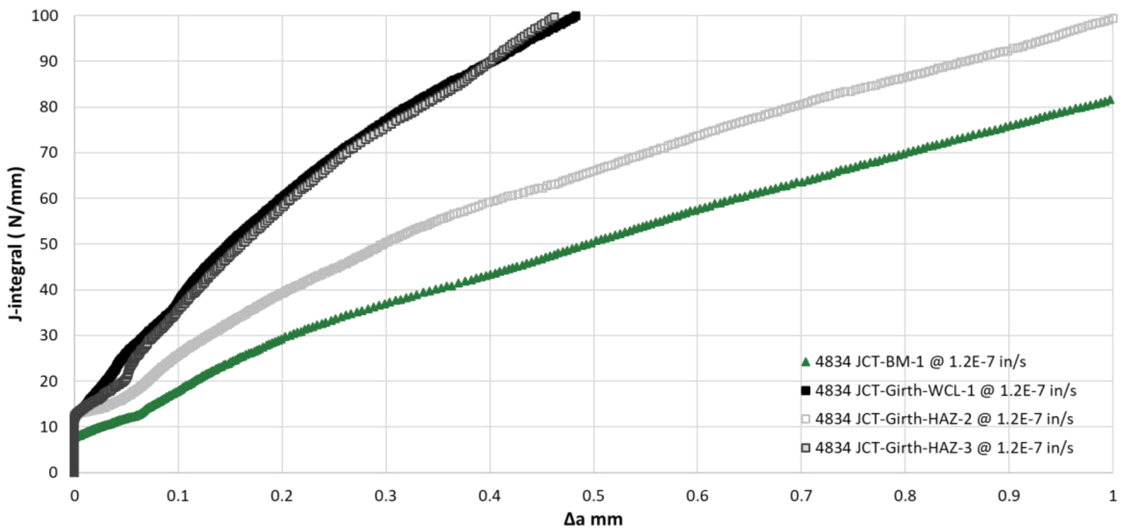

Figure 35. J-R curves for X46 specimens removed from the base metal, GWCL and GWHAZ. Shown here are results from only one CT specimen at each location.

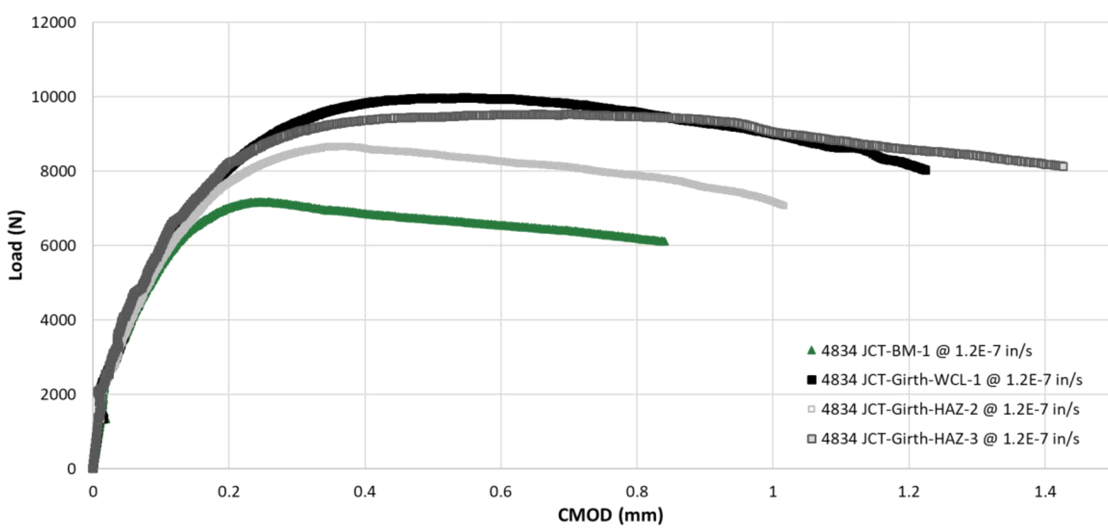

Figure 36. Load versus CMOD for X46 1964 specimens removed from the base metal, GWCL, and GWHAZ locations.

Table 6. Comparison of Fracture Toughness and stress intensity values from selected points on the testing curves for samples from X46.

Sample ID	Sample Location	$J_{0.0mm}$ (N/mm)	$J_{0.2mm}$ (N/mm)	$J_{Max\ load}$ (N/mm)	$K_{J0\text{-}H}$ (MPa√m)	$K_{J0.2\text{-}H}$ (MPa√m)	$K_{JMax\ Load\text{-}H}$ (MPa√m)
BM-1	Base metal	7.8	29.7	27.1	41.7	81.4	77.7
GWCL-1	Girth weld – weld centerline	12.3	60.2	94.0	52.3	115.8	144.7
GHAZ-2	Girth weld – heat affected zone	12.6	39.4	49.1	52.9	93.7	104.6
GHAZ-3	Seam weld – heat affected zone	11.8	58.2	123.0	51.3	113.9	165.5

Analysis of the J-R curves, Load vs. CMOD and post test assessment of the fracture surfaces suggest the following:

- [redacted]
- [redacted]
  - [redacted]

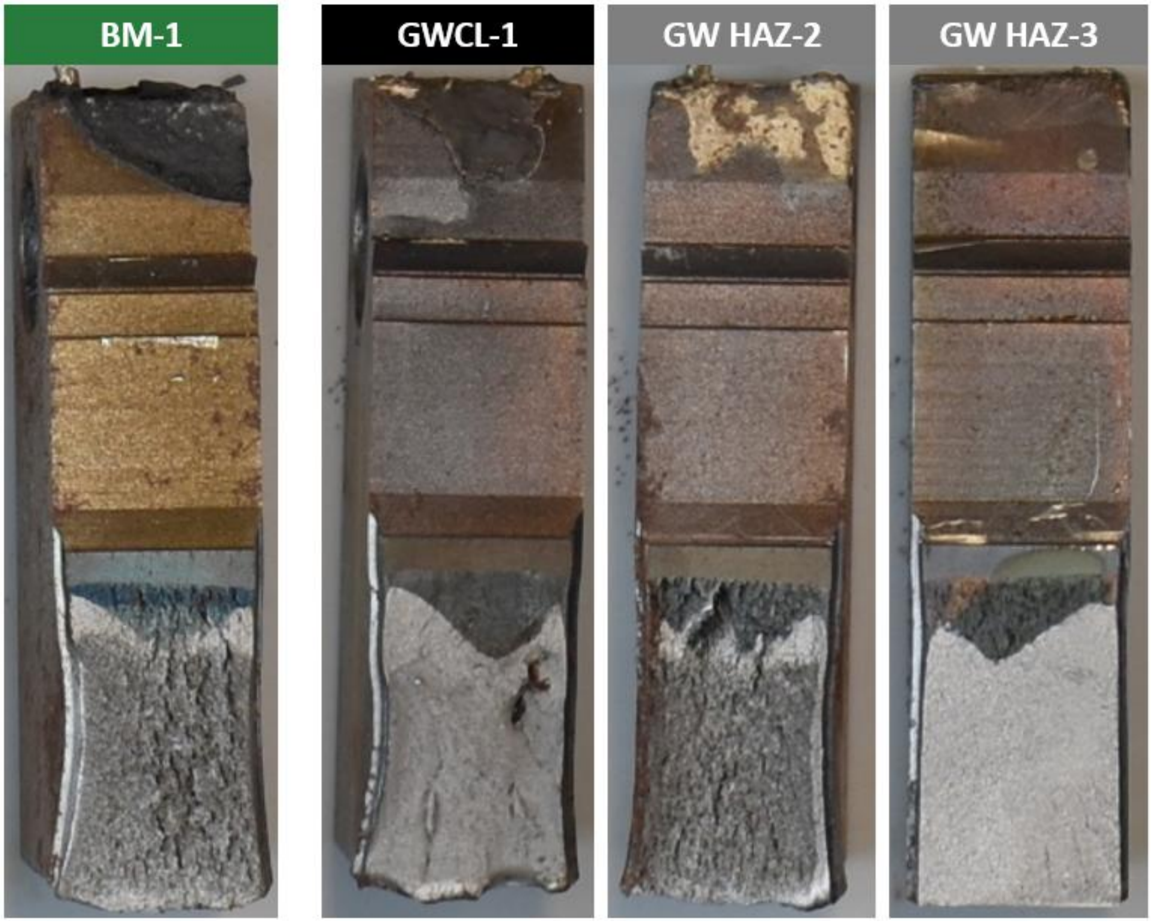

Figure 37. Post test fracture surfaces of base metal, GWHAZ and GWCL specimens from X46.

This analysis also showed that:

- Measured $K_{J0\text{-}H}$ values were similar for the GWLC and GWHAZ samples, ranging from 51.3 and 52.9 MPa√m, but a considerably lower $K_{J0\text{-}H}$ value (41.7 MPa√m) was recorded for BM-1, Table 6.
  - Slopes of the J-R curves varied from steep for GWCL-1 and GW-HAZ-2 (which were nearly identical) to comparatively shallow for BM-1.
  - GWCL-1 and GW-HAZ-2 had resulting $K_{J0.2\text{-}H}$ values >100 MPa√m, whereas BM-1 had a $K_{J0.2\text{-}H}$ value of 81.4 MPa√m.
  - Analysis of the Load vs. CMOD data along with the J-R data indicated that the $J_{Max\ Load\text{-}H}$ for BM-1 occurred at a Da value of 0.18 mm, corresponding to a $K_{JMax\ Load\text{-}H}$ of 77.7 MPa√m, which is below the measured value for MPa√m for $K_{J0.2\text{-}H}$.

6.5. Results for Tests on Samples from X65, 1988

The J-R fracture resistance curves for sample X65 1988 are shown in Figure 38 with the Load CMOD curves presented in Figure 39.

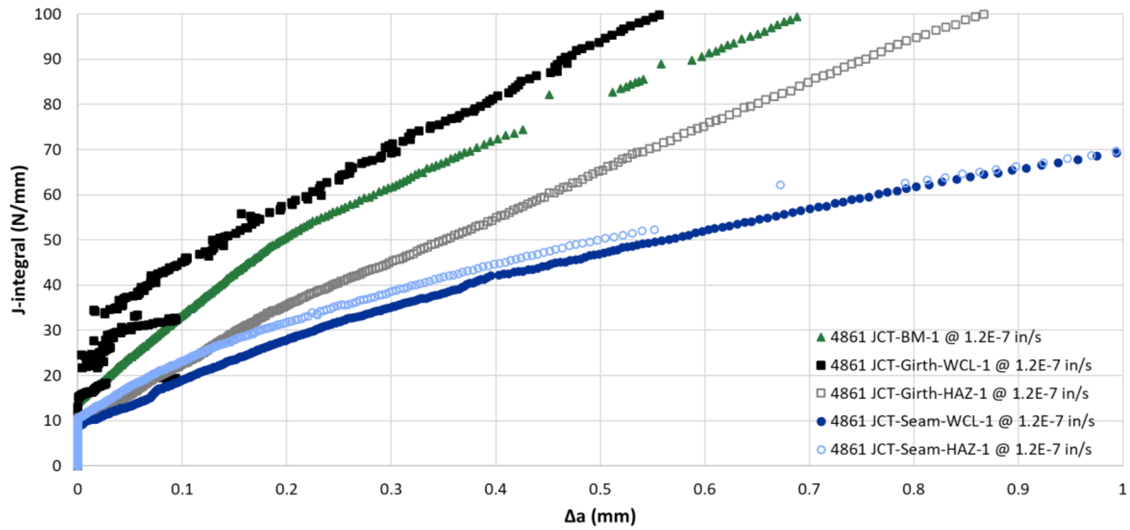

Figure 38. J-R curves for X65 1988 specimens removed from the base metal, GWCL, GWHAZ, SWCL and SWHAZ. Shown here are results from only one CT specimen at each location.

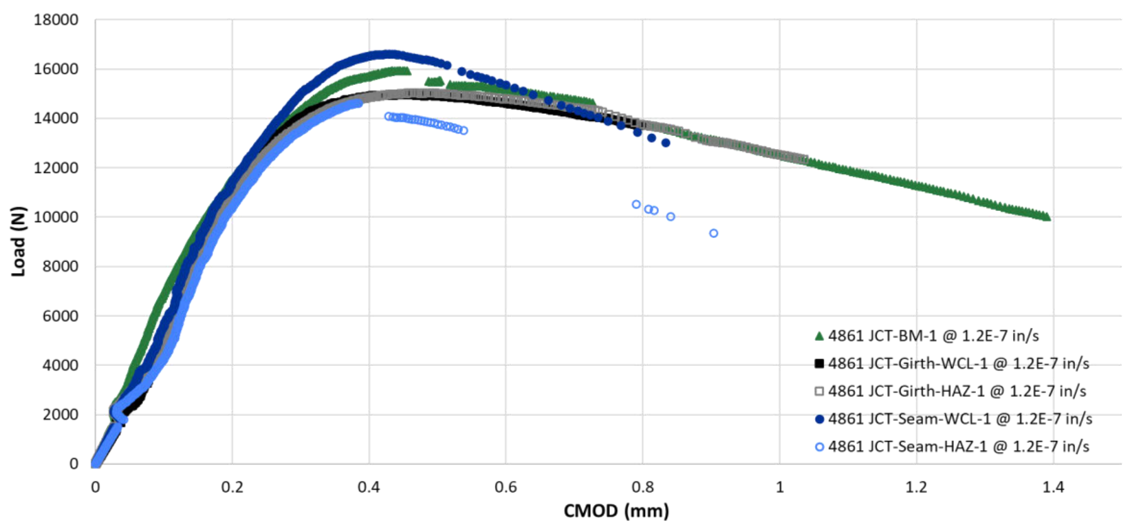

Figure 39. Load versus CMOD for X65 1988 specimens removed from the base metal, GWCL, GWHAZ, SWCL and SWHAZ locations.

Table 7. Comparison of Fracture Toughness and stress intensity values from selected points on the testing curves for samples from X65, 1988

Sample ID	Sample Location	$J_{0.0mm}$ (N/mm)	$J_{0.2mm}$ (N/mm)	$J_{Max\ load}$ (N/mm)	K_{J0-H} (MPa√m)	$K_{J0.2-H}$ (MPa√m)	$K_{JMax\ Load-H}$ (MPa√m)
BM-1	Base metal	14.1	50.7	72.3	56.0	106.3	126.9
GWCL-1	Girth weld – WCL	13.0	57.8	68.6	53.7	113.5	123.6
GHAZ-1	Girth weld – HAZ	10.4	35.7	70.7	48.1	89.1	125.5
SWCL-1	Seam weld – WCL	9.0	27.7	67.1	44.7	78.5	122.3
SHAZ	Seam weld - HAZ	10.5	31.9	52.3	48.3	84.2	108.0

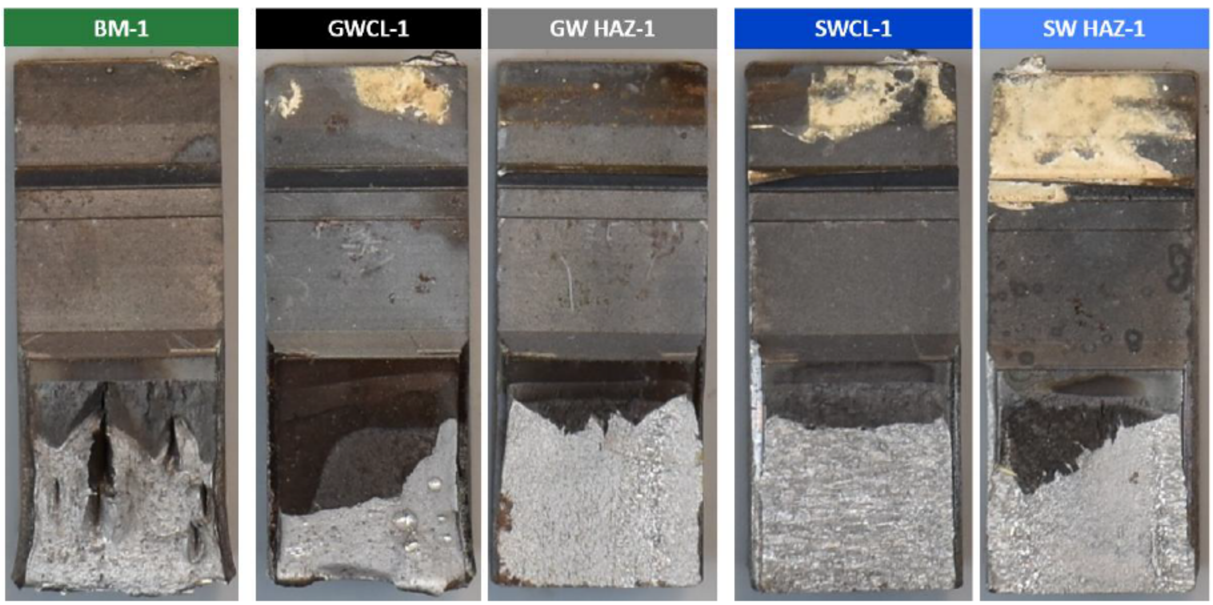

Figure 40. Post test fracture surfaces of base metal, GWHAZ and SWHAZ specimens from X65 1988.

Analysis of the J-R curves, Load vs. CMOD and post test assessment of the fracture surfaces suggest the following:

- With the exception of SWCL-1, all samples in this data set had irregular crack fronts
- Deep secondary cracking is evident on the fracture surface of BM-1, particularly in the region of fast fracture (i.e., not in the hydrogen tested region).
- Although no cross-sectional metallography was performed, clear changes in the fracture appearance are evident in GW-HAZ-1 and SW-HAZ-1 indicating that cracking progressed through different microstructures within the sample thickness.

- Measured K_{J0-H} values were somewhat variable with the lowest value (44.7 MPa√m) recorded from SWCL and the highest value (56.0 MPa√m) for BM-1.
  - The J-R curve for GWCL-1 was very irregular within the range Δa = 0.0 to 0.1 mm. The source of the data scatter is unclear but may be related to the irregular crack propagation path or weld porosity.
  - The J-R curve for BM-1 exhibits a very steep slope to Δa = 0.2 mm, then follows that of GWCL-1 and GW-HAZ-1
  - J-R curves and resulting data for SWCL-1 and SWHAZ were very similar, yet the fracture features in hydrogen gaseous were very different. This difference appears to be a consequence of crack propagation through the different microstructures. It is also interesting to note that SWCL-1 exhibited the highest maximum load, while SW-HAZ-1 exhibited the lowest maximum load.

6.5 Concluding Comments

Post test examination of fracture toughness samples tested in hydrogen gas is essential for determining whether the validity criteria identified in the applicable code was met. The results of the posttest examination also provide insights into how the cracking initiated and propagated within the region of interest, namely Δa = 0.0 to 0.2 mm.

[redacted]

- [redacted]
  - [redacted]
  - [redacted]

7. Discussion

This discussion section considers an overall assessment of the results of the study with particular emphasis on potential influences of repurposing to include the transmission of hydrogen. The results of the focused study described earlier in this report are considered with respect to other work. Available work from reports and publications is discussed as the information is relevant to the evaluation being undertaken by NTS with regard to the behaviour of gas transmission pipes repurposed for hydrogen service. Finally, recommendations are provided which outline potential future work which should be undertaken to reduce uncertainty in assessing performance in hydrogen.

The challenges involved in decision making regarding the repurposing of pipelines for hydrogen service are considered. The challenges include:

- *Fracture testing and then performing analysis of the test data to document materials properties in hydrogen*. Because testing standards and recent reviews are available, these technical points may seem inappropriate. However, there is at least some uncertainty regarding the selection of specimen geometry, the influence of trace elements in the test gas (e.g., oxygen) on behaviour and the value of displacement which provides the representative toughness.
- *Obtaining meaningful results from regions considered most susceptible to hydrogen embrittlement.* It is generally considered within the pipeline industry that material hardness is an indicator of susceptibility to hydrogen embrittlement. For example, ASME B31.12 includes language that components which will be used in hydrogen service should have a hardness below 250 HV and PRCI's Consensus Engineering Requirements document published in 2024, which is expected to be incorporated into ASME B31.8 in 2026, stipulates a hardness limit of 275 HV for pipeline steel components.
- *Measurement of properties such as fracture toughness for steel welds.* It is well established that weld manufacture involving melting and solidification will result in complexities linked to heterogeneous microstructures, welding residual stresses, and in many cases weld defects. Taking these factors (and other variables) into account empirically is not straightforward.
- *Predictions of in-service component performance are often made using formulae-based rules.* However, these approaches tend to be simplistic and, by necessity, include assumptions which are intended to ensure conservatism. More realistic estimates of behaviour should be made using science-based engineering models which have been validated from comparison with component performance.

7.1 Testing and Analysis

Research is on-going to establish the value of displacement which should be used to obtain component relevant values of fracture toughness from laboratory tests. Data selected from the current experimental results indicate that the fracture toughness at a displacement of 0.2 mm, $K_{J0.2-H}$, was relatively similar for X60A, X60B and X80, regardless of the location from which the specimens were removed, Table 8.

Table 8. Fracture resistance values at Δa = 0.0mm and Δa = 0.2mm for X60A, X60B and X80 pipeline steels tested in 69 bar hydrogen gas.

Sample	Location	K_{J0-H} (MPa√m)	$K_{J0.2-H}$ (MPa√m)
X60A	Base metal	47.2	88.8
	GWCL	51.7	101.6
	GHAZ	56.4	104.5
X60B	Base metal	51.0	104.3
	GWCL	51.9	118.9
	GHAZ	44.4	112.2
X80	Base metal	62.5	104.7
	GWCL	59.3	120.2
	GHAZ	58.0	112.5

Likewise, as shown in Figure 41, the general shapes of the J-R curves for all three specimens removed from X60A and all three specimens removed from X60B showed very similar trends. Considering that each specimen within a dataset was supposed to represent a specific region from the weldment (i.e. base metal, HAZ and weld metal), this result may seem surprising. However, if the variability in composition and hardness through the thickness of the specimens at the locations representative of the WCL and HAZ are considered, perhaps the results are in line with expectation. Detailed characterization of weld cross sections identified that welding consumables with different compositions were likely used in the root, fill and/or cap passes, resulting in variable hardness (and mechanical properties) through the thickness. Thus, fracture toughness results from the weld centreline represent a composite response from all constituent microstructures and features. Furthermore, attempts to accurately measure the fracture resistance within the HAZ of a girth weld presents inherent challenges due to typical weld geometries and extreme changes in microstructure and mechanical properties within the different regions of the HAZ.

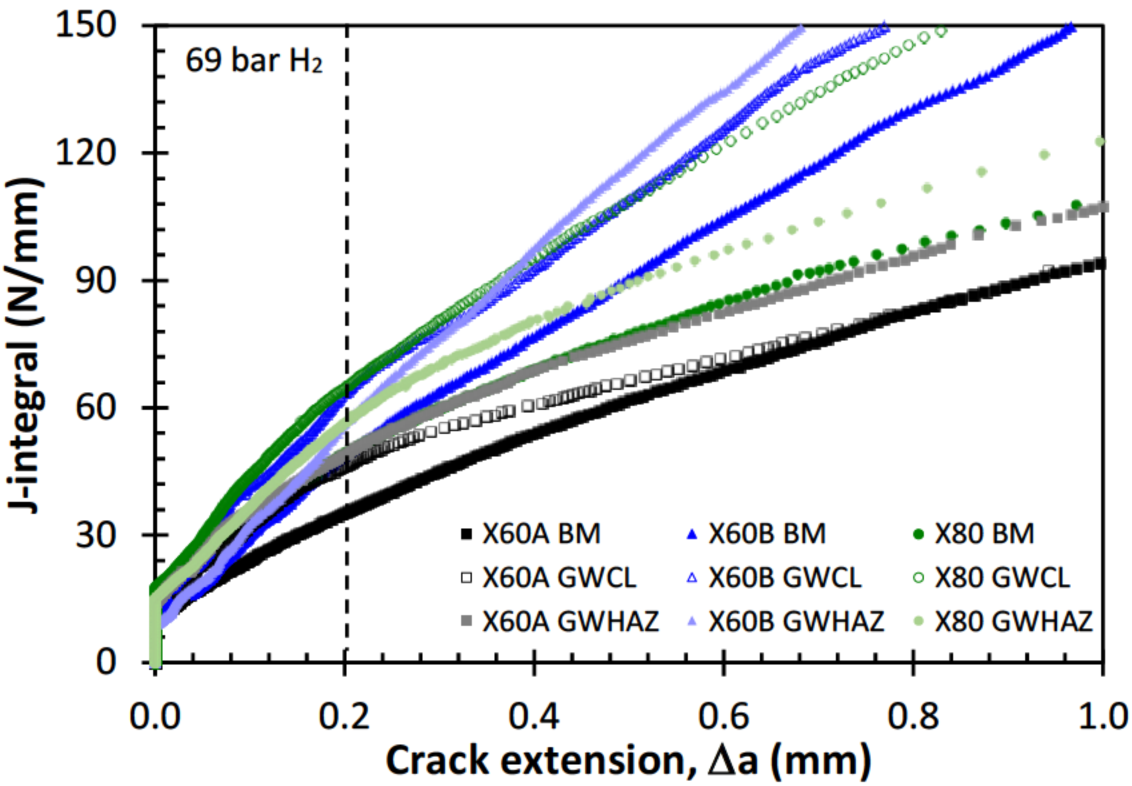

Figure 41. J-R curves for X60A, X60B and X80 pipeline steels fracture toughness tested in 69 bar H_2 gas.

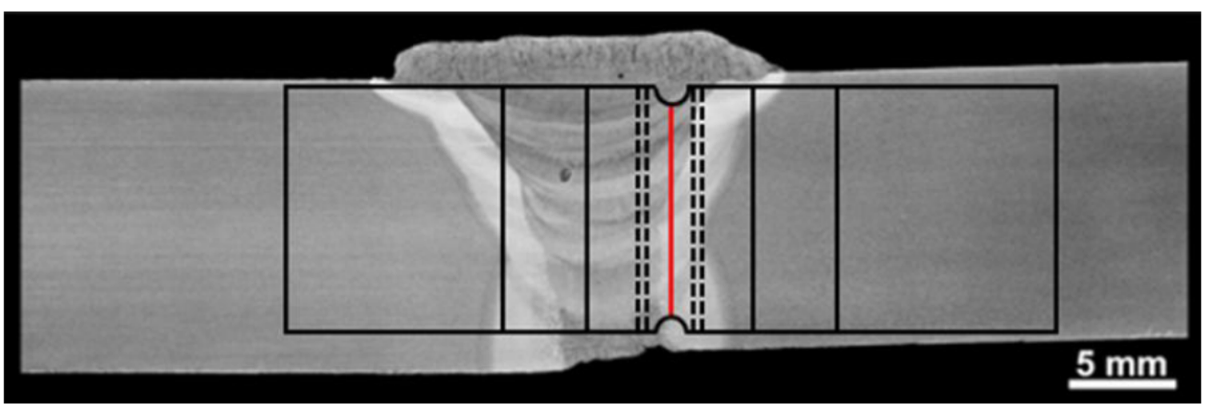

Figure 42. Sketch of a typical CT specimen geometry superimposed on a metallographic cross section through the X60A girth weld.

Figure 42 shows a schematic illustration of a CT specimen superimposed on the macrograph through the X60A weld. Consideration of this figure shows that placing a notch anywhere within the HAZ inevitably results in crack growth contributions from the weld metal, and depending on weld geometry, possibly from the base metal. The course-grained heat-affected zone is generally regarded as the region that is most susceptible to hydrogen embrittlement. However, the accepted methodology for testing HAZ specimens in girth welds does not unambiguously provide meaningful data from the most critical region of the weld. While it is possible that a small portion of the coarse-grained HAZ is tested, in the end, the fracture response will be measured from a composite microstructure and therefore is likely not representative of worst-case fracture properties, nor representative of component behaviour in a hydrogen pipeline.

The inverse relationship between hardness/strength, toughness and hydrogen embrittlement susceptibility is well established. More and more data are becoming available, which is continually adding to the knowledge base. The data presented in Figure 43 covers samples with hardness over the range of 140 HV to about 460 HV. It is clear that fracture toughness values taken from tests on base metal samples are not appropriate for assessing the behaviour of welds. Moreover, even experiments conducted on samples taken from the weld do not necessarily produce valid data. Challenges with testing samples extracted from line pipe welds include the specimen size, and the fact that they necessarily encompass a wide range of hardness/microstructural regions.

Recently, EPRI have been collaborating with a number of research organizations to apply specialist heat treatment to permit manufacture of typical specimens from microstructure relevant to welds. Data from these HAZ relevant microstructures are included in Figure 43. As $K_{J0\text{-}H}$ refers to point at which a stable crack initiates, the values obtained at this position are typically lower than those measured at $K_{J0.2\text{-}H}$. Figure 43 shows that the trends in behaviour for both fracture toughness values are similar with respect to the measured hardness. Thus, it appears that there is consistency in the trends obtained. It should, however, be emphasized that in some fracture tests on brittle structures, such as those which can be found in weld HAZs, the displacement of Δa = 0.2 mm is not achieved before failure. Thus, care should be exercised in identifying the appropriate toughness values to apply for assessment of components.

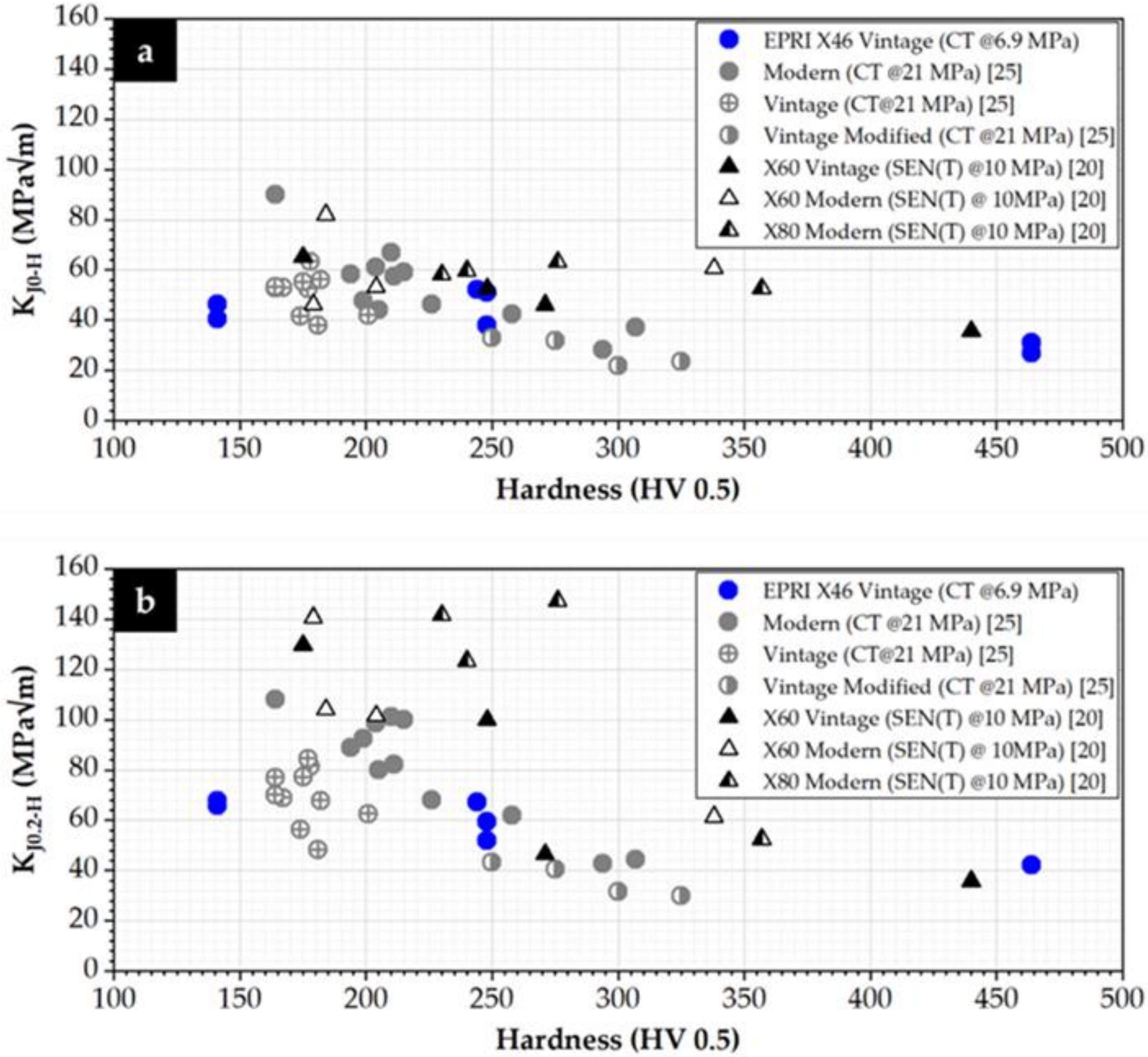

Figure 43. Fracture toughness in gaseous hydrogen as a function of hardness for crack extensions of 0.0 mm (a) and 0.2 mm (b). Data from the present work and previously published data, adapted from Refs. [9,26], are included for comparison. Note that circles represent testing performed on CT specimens whereas triangles represent testing performed on SEN(T) specimens.

7.2 Application of Models to Estimate In-service Performance

It is emphasized in the discussion at recent expert meetings and in PRCI documentation that empirically derived assessment models are not appropriate for use in hydrogen service. The challenges involved are highlighted in Figure 43. The data presented in Figure 43 shows that the initiation toughness values (K_{J0-H}) in hydrogen may be as low as 20 MPa√m in vintage steels that exhibit high hardness [25]. This is lower than the minimum fracture toughness value of 55 MPa√m recommended for pipeline steels in ASME B31.12 [3]. As shown in Figure 43b, even at 0.2 mm crack extension ($K_{J0.2-H}$), recorded fracture toughness values in hydrogen for vintage pipeline steels that have been heat-treated to produce weld relevant microstructures with hardness values above

250 HV (i.e., closed black triangles [9], semi-closed grey circles [25], and closed blue circles) are typically below 50 MPa√m.

While not explicitly shown, these figures illustrate that there is little difference in the toughness values for the selected levels (i.e., Δa = 0.0 mm and Δa = 0.2 mm) of displacement because the J-R curves are flat. Recent testing on homogeneous samples indicates that this behaviour was typically observed in samples with large prior austenite grain size and were relatively brittle. These findings are consistent with observations that pipeline steels with localized regions of high hardness are susceptible to hydrogen embrittlement. Weld HAZs that contain coarse-grained martensite microstructures are therefore likely to exhibit low toughness in hydrogen service. It is apparent then that weld procedures should consider selection of weld profiles and parameters, including the size, heat input and sequence of weld bead placement, such that the welding thermal cycles minimize the extent of coarse prior austenite grains [9]. Optimization of welding procedures should also seek to ensure that welds, including the HAZ, are not significantly understrength. These issues were identified as contributory factors to failures of in-service pipelines (PRCI project MATH - 5-3B).

Because of the complexities and the uncertainties involved, it is very unlikely that laboratory testing alone will provide a complete engineering assessment of pipeline performance in hydrogen service. Instead, relevant material data in combination with validated models of performance offers real potential to provide the answers necessary for safe, reliable, and affordable transmission of hydrogen [9,26,27]. Recent models have been developed using a multi-stage approach that couples a thermo-metallurgical-mechanical model with a deformation-diffusion-fracture model. In the first stage of the simulation framework, local fractions of microstructural constituents were predicted based on steel composition and welding parameters. The resulting phase fraction maps were then used to define heterogeneous properties that were employed in structural integrity assessments using an elastoplastic phase field fracture model. Selected engineering outcomes achieved using these scientifically sound models include:

- An accurate characterisation of residual stresses can be decisive in determining the failure mode. In the absence of pre-existing defects, models which include residual stresses predict a significant reduction in fracture pressure.
- The maximum admissible pressure was found to be very sensitive to the size, location and orientation of pre-existing defects. Model predictions of fracture pressure when 2 mm (0.079 in) long defects were included within a metallurgically hard HAZ were reduced by 50% compared to defect free structures.

Recent experimental research developed controlled heat treatments which were successful in reproducing the hardness levels and microstructures observed in the HAZ of existing natural gas pipelines. These heat treatments were used to produce test specimens with homogeneous microstructures. Subsequently, fracture experiments conducted in air and pure H_2 gas at 100 bar (1450 psi) revealed a reduced fracture resistance and higher hydrogen embrittlement susceptibility of the HAZ microstructures. In the worst-case, initiation toughness values as low as 32 MPa√m (29 ksi√in) were measured. The findings emphasize the need to adequately consider the influence of microstructure and hard, brittle zones within the HAZ.

8. Recommendations Related to Repurposing the NTS System for Hydrogen Service

The concept of hydrogen pipelines is not new and today, there are approximately 2800 mi (4,500 km) of dedicated hydrogen pipelines around the world. While hydrogen transmission through pipelines has been relatively limited in comparison with natural gas, the service experience has generally been very good, indicating that the hydrogen can be safely and reliably transported. However, as interest continues to grow and the concept of repurposing existing natural gas pipelines to hydrogen service becomes reality, it is important to recognize the differences not only in the physical characteristics between natural gas and hydrogen, but also the differences in the design and operation of the pipelines. Existing hydrogen pipelines are comparatively much smaller in diameter, operate at lower pressures, are typically subject to fewer pressure fluctuations than natural gas pipelines, and are deliberately constructed of relatively low strength materials (typically ≤X52) to minimize susceptibility to hydrogen embrittlement.

There is no current understanding of what lower bound properties can reasonably be assumed for use in assessments of the performance of pipeline welds in hydrogen. As the effects of hydrogen embrittlement on different types of line pipe steels are not fully elucidated, it is possible that existing lower bound property assumptions may not be conservative in all cases. Benefit would be forthcoming if there was clarification of how to undertake testing to measure worst case fracture toughness. To achieve this goal, it is recommended that a focussed experimental program be undertaken that includes performing specialist heat treatments to simulate microstructures relevant to the HAZ of critical welds in the NTS system followed by fracture toughness testing in hydrogen. Furthermore, at least a selection of these tests should be terminated at low displacement (prior to failure) to evaluate initiation and stable crack growth in hydrogen. In all cases, testing should be followed by post test laboratory characterization.

Details of inspection and characterization of the defects in the NTS pipeline system are not known by EPRI staff. However, it is apparent that defects, particularly those of a linear character will promote fracture. It is recommended that analysis using validated models is undertaken to estimate the influence of defects on fracture mode and pressure for components in the NTS system.

If future plans include the manufacture of new pipelines for the transmission of hydrogen gas, the applicable codes such as ASME B 31.12 [3] should be followed. Service experience has shown that new construction to these requirements will result in safe service.

9. References

[1] "Clean Power 2030: Action Plan: A new era of clean electricity," 2024. Available online: www.gov.uk/desnz (accessed January 13, 2026)

[2] *The Climate Change Act 2008 (2050 Target Amendment) Order 2019*. 2019. Available online: https://www.legislation.gov.uk/ukdsi/2019/9780111187654 (accessed January 13, 2026).

[3] American Society of Mechanical Engineers (ASME). Code for Pressure Piping, B31 Standard, ASME B31.12: Hydrogen Piping and Pipelines. ASME, 2023.

[4] Institution of Gas Engineers and Managers (IGEM). IGEM-TD-1 Ed 6 Supplement 2: Communication 1849 – High Pressure Hydrogen Pipelines. IGEM, 2021.

[5] British Standards Institute (BSI). BS 7910: Guide to Methods for Assessing the Acceptability of Flaws in Metallic Structures. BSI, 2019.

[6] American Petroleum Institute (API). API 579-1/ASME FFS-1: Fitness-For-Service. API, 2021.

[7] Canadian Standards Association (CSA Group). ANSI/CSA CHMC 1-2014 (R2023): Test Methods for Evaluating Material Compatibility in Compressed Hydrogen Applications - Metals. CSA Group, 2014.

[8] *EPRG Draft best practice guidelines for small scale fracture toughness testing is hydrogen gas of carbon steel pipeline material*. EPRG, Duisburg, Germany: 2024. https://www.eprg.net/fileadmin/EPRG_Dokumente/EPRG-Guidelines-Rev-4a_01.pdf.

[9] Chalfoun, D.R.; Parker, J.; Gagliano, M.; Martínez-Paneda, E. Tailored Heat Treatments to Characterize the Fracture Resistance of Critical Weld Regions in Hydrogen Transmission Pipelines. Int. J. Hydrog. Energy 2025, 192, 152347.

[10] International Organization for Standards (ISO). ISO 18265 (2013): Metallic materials – Conversion of hardness values, ISO, 2013.

[11] American Petroleum Institute (API). API Specification 5L (46th Edition): Specification for Line Pipe. API, 2018/2025.

[12] His_1: Steel and Pipe making in Europe - Supporting Assessment of Legacy Gas Pipeline Steels to Hydrogen Embrittlement Effects NIA project.

[13] National Gas Line Pipe Specs Data v.0.

[14] Pol_29: GC/PS/P2 - DRAFT - STANDARD FOR FIELD WELDING OF STEEL PIPELINES - The Gas Council – Apr-1969.

[15] Pol_8 : GC/PS/P.2 - DRAFT - SPECIFICATION FOR FIELD WELDING OF STEEL PIPELINES - The Gas Council – Dec-1970.

[16] Pol_18 BGC/PS/P2 - SPECIFICATION FOR FIELD WELDING OF STEEL PIPELINES AND INSTALLATIONS FOR HIGH PRESSURE GAS TRANSMISSION - British Gas – Apr-1981.

[17] Pol_21 BGC/PS/P2 - DRAFT - SPECIFICATION FOR WELDING OF LAND PIPELINES AND INSTALLATIONS DESIGNED TO OPERATE AT PRESSURES ABOVE 7 bar (INCORPORATING BS 4515) - British Gas – Jul-1991.

[18] Pol_47 BGC/PS/P8 - SPECIFICATION FOR SHOP FABRICATION and INSPECTION PROCEDURES FOR PRESSURE REDUCTION AND OFFTAKE STATIONS - Issue 1 - British Gas – Oct-1975.

[19] British Standards Institute (BSI). BS 4575:1984 – Fluid Power Transmission and Control Systems. Guide for Hydraulic Equipment and Systems. BSI, 1984.

[20] Rep_1: Mechanical and fatigue properties of Pre-1972 Girth welds.

[21] Pol_11: PS/P2 - DRAFT - SPECIFICATION FOR FIELD WELDING OF STEEL PIPELINES FOR HIGH PRESSURE GAS TRANSMISSION - British Gas – Nov-1973.

[22] Rep_16: Summary of Integrity and Risk Assessment Studies on Low Toughness Pipelines Operated by National Grid UKT – May-1976.

[23] British Standards Institute (BSI). BS 7610:1971 – Fatigue design and assessment of steel structures. 1971.

[24] ASTM International. ASTM E1820-23a: Standard Test Method for Measurement of Fracture Toughness. ASTM, 2023.

[25] Ronevich J., Agnani M., Gagliano M., Parker J., and San Marchi C., "Influence of Hardness on Hydrogen-Assisted Fracture in Pipeline Steels," Proceedings of the 2024 14th International Pipeline Conference, Calgary, Alberta, Canada. 2024. https://doi.org/10.1115/IPC2024-133937.

[26] Mandal, T.K.; Parker, J.; Gagliano, M.; Martínez-Paneda, E. Computational Predictions of Weld Structural Integrity in Hydrogen Transport Pipelines. Int. J. Hydrog. Energy 2025, 136, 923–937.

[27] Wijnen, J.; Parker, J.; Gagliano, M.; Martínez-Paneda, E. A Computational Framework to Predict Weld Integrity and Microstructural Heterogeneity: Application to Hydrogen Transmission. Mater. Des. 2025, 249, 113533. https://doi.org/10.1016/j.matdes.2024.113533.